CSIRO PUBLISHING

Exploration Geophysics
http://dx.doi.org/10.1071/EG15112

Improved reservoir characterisation using fuzzy logic platform: an integrated petrophysical, seismic structural and poststack inversion study

Muhammad Kamran Jafri[1,2] Aref Lashin[3,4,6] El-Khedr Hassan Ibrahim[1,5]
Kamal A. Hassanein[1] Nassir Al Arifi[1] Muhammad Naeem[1]

[1]King Saud University, College of Science, Department of Geology and Geophysics, PO Box 2455, Riyadh 11451, Saudi Arabia.
[2]Bahria University, Department of Earth and Environmental Sciences, Islamabad 44000, Pakistan.
[3]King Saud University, College of Engineering - Petroleum and Gas Engineering Department, PO Box 800, Riyadh 11421, Saudi Arabia.
[4]Benha University, Faculty of Science - Geology Department, Benha 13518, Egypt.
[5]Mansoura University, Faculty of Science - Geology Department, Mansoura 35516, Egypt.
[6]Corresponding author. Email: aref70@hotmail.com

Abstract. There is a tendency for applying different integrated geophysical approaches for better hydrocarbon reservoir characterisation and interpretation. In this study, petrophysical properties, seismic structural and poststack seismic inversion results are integrated using the fuzzy logic AND operator to characterise the Tensleep Sandstone Formation (TSF) at Powder River Basin (PRB), Wyoming, USA. TSF is deposited in a coastal plain setting during the Pennsylvanian era, and contains cross-bedded sandstone of Aeolian origin as a major lithology with alternative sabkha dolomite/carbonates. Wireline logging datasets from 17 wells are used for the detailed petrophysical evaluation. Three units of the TSF (A-sandstone, B-dolomite and B-sandstone) are targeted and their major rock properties estimated (i.e. shale/clay volume, V_{sh}; porosity, ϕ_{Eff}; permeability, K; fluid saturations, S_w and S_H; and bulk volume water, BVW). The B-sandstone zone, with its petrophysical properties of 5–20% effective porosity, 0.10–250 mD permeability and hydrocarbon potential up to 72%, is considered the best reservoir zone among the three studied units. Distributions of the most important petrophysical parameters of the B-sandstone reservoir (V_{sh}, ϕ_{Eff}, K, S_w) are generated as GIS thematic layers.

The two-dimensional (2D) and three-dimensional (3D) seismic structural interpretations revealed that the hydrocarbons are entrapped in an anticlinal structure bounded with fault closures at the west of the study area. Poststack acoustic impedance (PSAI) inversion is performed on 3D seismic data to extract the inverted acoustic impedance (AI) cube. Two attribute slices (inverted AI and seismic amplitude) were extracted at the top of the B-sandstone unit as GIS thematic layers. The reservoir properties and inverted seismic attributes were then integrated using fuzzy AND operator. Finally, a fuzzy reservoir quality map was produced, and a prospective reservoir area with best reservoir characteristics is proposed for future exploration. The current study showed that integration of petrophysical, seismic structural and poststack inversion under a fuzzy logic platform can be used as an effective tool for interpreting multiple reservoir zones.

Key words: fuzzy logic, petrophysical analysis, reservoir characterisation, seismic inversion, Teapot Dome, Tensleep.

Received 27 October 2015, accepted 29 April 2016, published online 23 June 2016

Introduction

Effective description of petroleum reservoirs holds great importance in hydrocarbon exploration as well as reservoir management and development plans. Reservoir characterisation is an integrated approach to describe the reservoir as subunits based on its rock properties (Amaefule et al., 1993). Well logs, cores, production or engineering data and seismic data can be integrated and used as an input to describe the reservoir characteristics. At any stage of hydrocarbon exploration to exploitation, well logs and three-dimensional (3D) seismic data can be integrated to efficiently characterise the reservoir for achieving economic benefits (Amigun and Bakare, 2013). Core data are of great importance and give direct measurement of rock properties compared to the wireline logs (Sneider and King, 1984; Amaefule et al., 1993).

Seismic data can be used in delineating the prevailing structural elements that affect the reservoir of interest and determining its exact subsurface geometry. The velocity of seismic waves depends mainly on the elastic and petrophysical properties (pore spaces, matrix type, fluid content, lithology content and type, etc.) of the studied rock units. The traveltimes (one- and two-way) and the average and interval velocities are very important parameters in velocity analysis due to their role in clarifying the boundaries of the different rock units and defining the acoustic subsurface characteristics of the study area, with special emphasis on the hydrocarbon-bearing sections (Gardner et al., 1974; Wang, 2001; Lashin and Abd El Aal 2004*a*, 2004*b*; Contreras et al., 2005; El-Mowafy and Marfurt, 2008; El-Naby et al., 2009; Lashin et al., 2011, 2014; AlMuhaidib et al., 2012; Lashin and El-Naby, 2014).

Recently, the awareness of quantitative seismic inversion, particularly acoustic impedance (AI) inversion, has increased considerably (Latimer et al., 2000; Vargas-Meleza et al., 2004; Pendrel, 2006; Russell and Hampson, 2006). Seismic data inversion is a renowned practice in the upstream petroleum sector that is used to refine structural interpretation, property prediction and reservoir characterisation. Seismic inversion is a special case of 'inverse problem' used to derive certain physical properties of the subsurface. The inversion problem is strictly linked to forward modelling (forward problem), which deals with resolving the data to be acquired for a given sequence of subsurface structures/formations.

This is done under the assumption of the physical laws ruling the phenomenon of interest (i.e. wave propagation, diffusion and potential field). As far as the seismic exploration is concerned, forward modelling is achieved using mathematical relationships to generate a seismic response of the subsurface geology through acoustic energy. Poststack acoustic impedance (PSAI) inversion can be grouped into two broad approaches: band-limited and broad-band inversion. Broad-band inversion includes the model based and sparse spike approaches that we adopted in this research (Russell and Toksöz, 1991).

The results of seismic inversion can be applied as an effective tool for enhanced reservoir development strategy. It has a greater resolution when compared to the input of real seismic data. This higher resolution is attained by the elimination of band-limited wavelet effects from actual seismic data (Pendrel and Van Riel, 1997; Savic et al., 2006; Latimer et al., 2000; Pendrel, 2001; Veeken and Da Silva, 2004; Russell, 2005; Al-Zuabi et al., 2011).

AI inversion is very useful to accomplish effective descriptions and characterisations of reservoir properties . AI can be obtained by the integration of data from different sources and can be closely associated to subsurface rock properties. AI can also be linked to geological investigation because it is a lithologic property instead of an interface property (Latimer et al., 2000; Lashin et al., 2011; Naeem et al., 2015).

Fuzzy logic is an overlay analysis approach that can be used for solving the suitability models or site selection issues. The basic principle of the fuzzy logic is that there are imprecisions in attributes and the spatial data geometry. Fuzzy logic (set theory and a fuzzy membership) can address such types of imprecisions, as well as pinpointing the favourable sites or zones in the suitability models (Esri, 2011, 2012). The principle of set theory and a fuzzy membership is defined on a scale of 0–1 for every class, and it defines the possibilities rather than probabilities (Kainz, 2010, chapt. 12; Esri, 2012). We applied the fuzzy AND operator to focus on the zones where all the input parameters point to the same high level reservoir potential.

This study aims to adequately integrate the petrophysical analyses, seismic structural and seismic inversion results in order to characterise the Tensleep sandstone reservoir. The main petrophysical properties of the reservoir and inverted

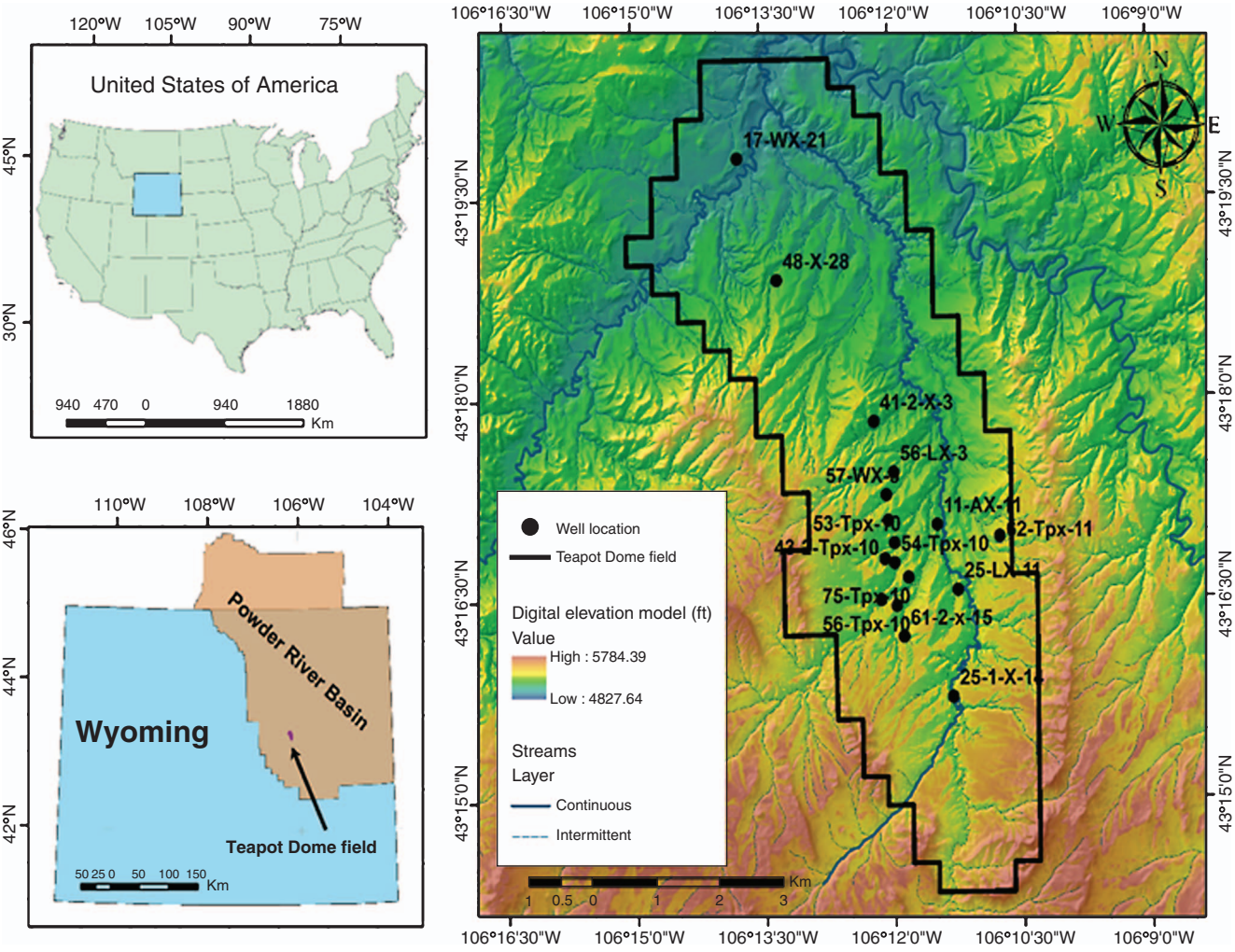

Fig. 1. Location map of the Teapot Dome field, PRB, Wyoming, USA.

seismic attributes are transformed into GIS thematic layers. These property layers are integrated using the fuzzy logic AND operator in ArcGIS fuzzy overlay tool. Finally, a fuzzy prediction map is generated for the best reservoir area that could be further used for hydrocarbon exploitation.

Exploration history and geologic setting

The Teapot Dome field is a faulted dome structure in the Salt Creek anticline present in the south-western portion of the Powder River Basin (PRB), north of Casper in Natrona County, Wyoming (Figure 1). The Teapot Dome is part of a basin margin anticline play of the PRB petroleum province (Dolton and Fox, 1995). The oil production from Teapot Dome started in 1908 from the 'Dutch' well. It flowed at a rate of 200 BOPD from the First Wall Creek sandstone. The Teapot Dome field was established as Naval Petroleum Reserve (NPR) in 1915 (Doll et al., 1995; Roth et al., 2005). Field operations at Teapot Dome were suspended for about 50 years due to a corruption scandal in the 1920s (Encyclopedia Britannica, 2014).

Field activity was resumed at Teapot Dome in 1976, and later in 1977, when it became a facility of US Department of Energy (DOE). Teapot Dome's production met its highest

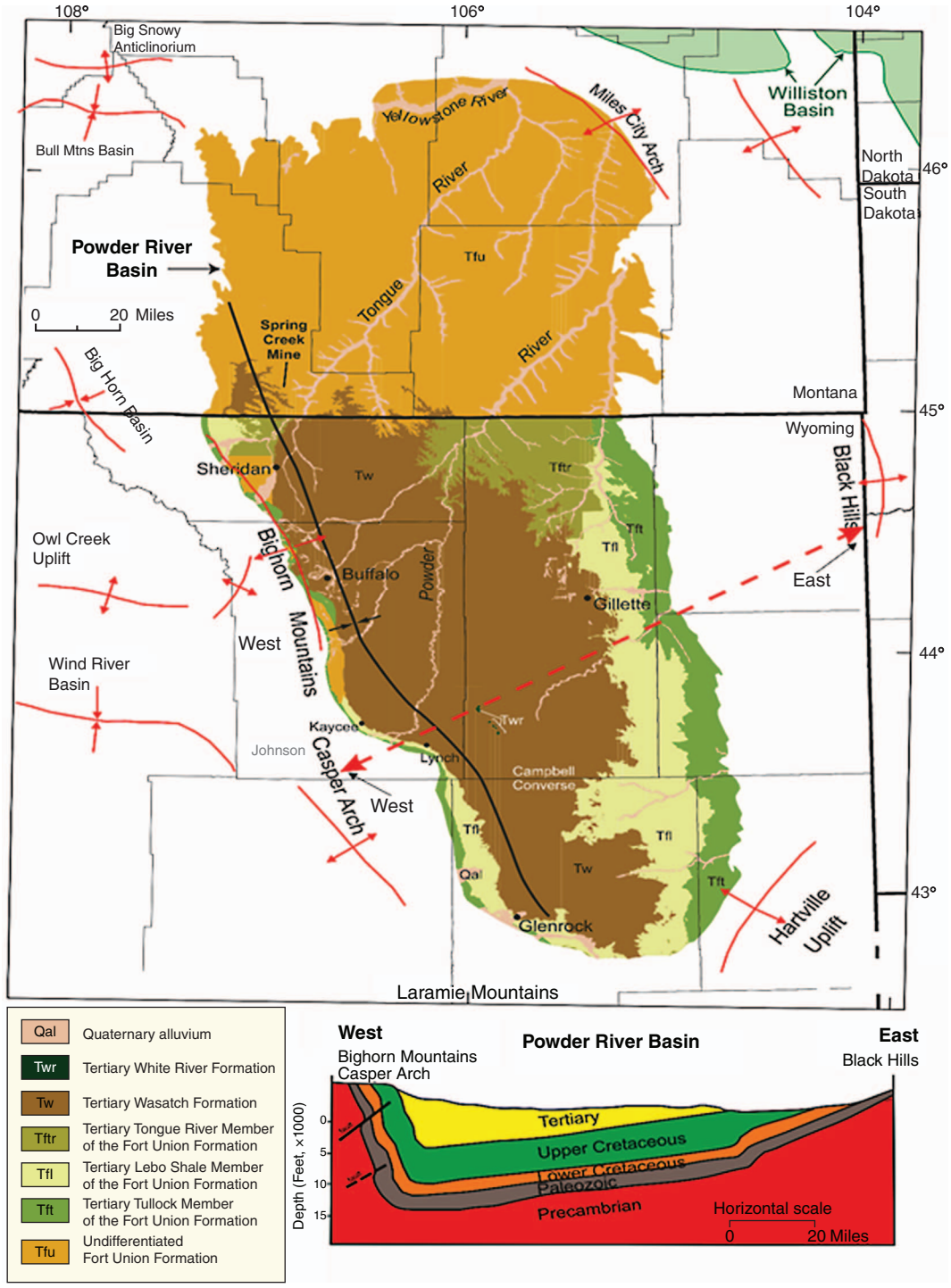

Fig. 2. Geological map showing the geology of the PRB and an east–west cross-section through the basin (modified from Jafri et al., 2016).

levels in 1981 and then started to decline progressively. This provoked the DOE to convert its facility into the Rocky Mountain Oil Testing Centre (RMOTC). The RMOTC is engaged in collaborating with the oil/gas sector, academic and research organisations to enhance domestic hydrocarbon production by field testing advanced technology (Roth et al., 2005). Overall, 233 wells had been drilled in the field before the operations were resumed in 1976. Oil production has targeted nine different reservoirs ranging from Pennsylvanian age Tensleep Sandstone Formation (TSF) to the Upper Cretaceous Shannon Sandstone. Drilling activity was increased to 1007 development wells and 90 exploratory wells in late 1990s. Among the development wells, 27 were aimed to test the potential of TSF. Two of these wells flowed at highest initial production rates compared

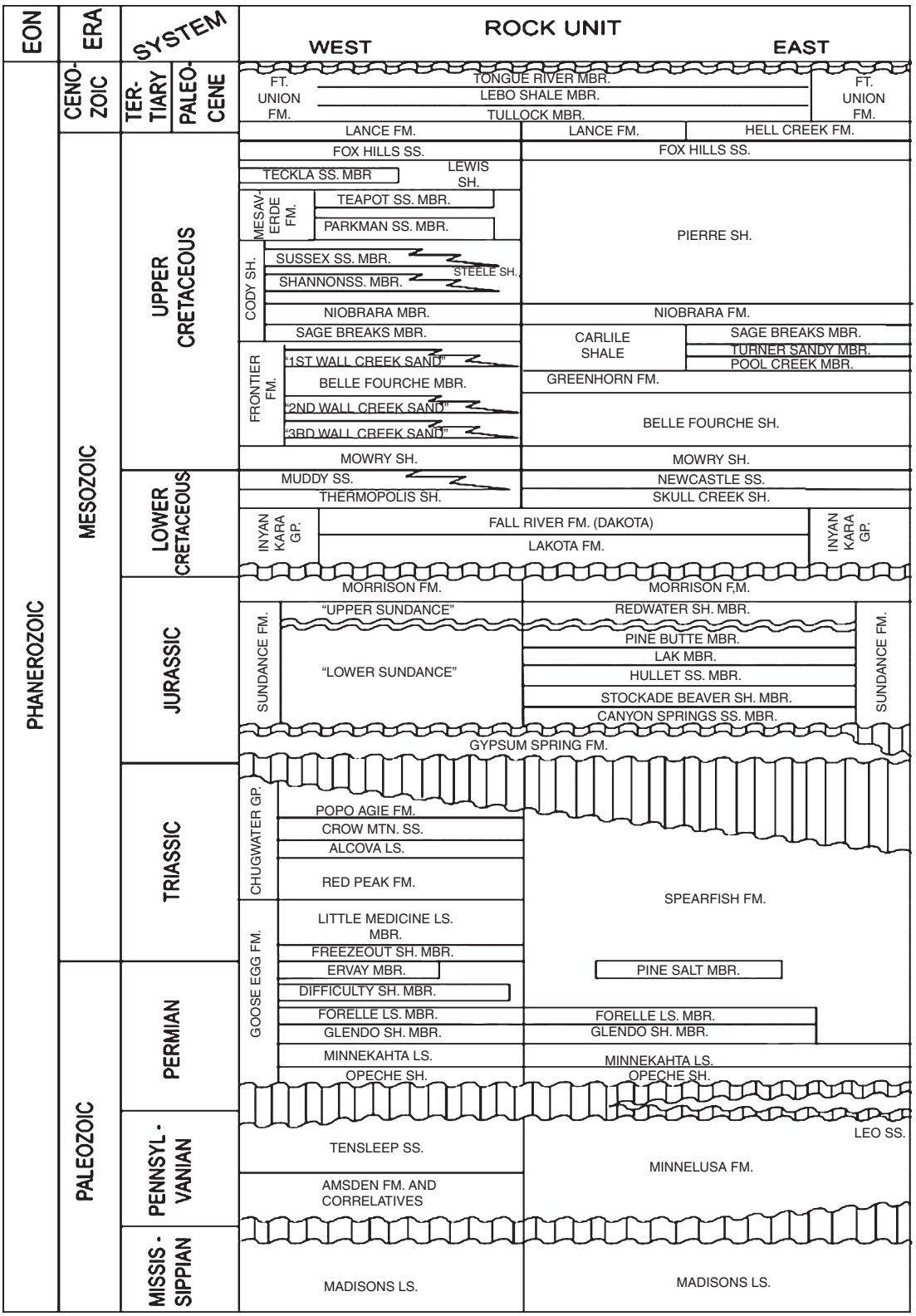

Fig. 3. General stratigraphic column at the Teapot Dome field (modified from Dolton and Fox, 1995).

to any of the wells in Wyoming at that time. In October 2003, Teapot Dome was established as a national geological carbon storage test centre (Friedmann et al., 2004).

The PRB was formed during the Laramide orogeny and contains thick successions of sedimentary strata, surrounded by successive uplifted mountains and basins from all sides (Figure 2) (Anna, 2009). The basin is an asymmetric syncline whose eastern flank near the Black Hills dips gently, while the western flank near Casper Arch dips more steeply (see cross-section in Figure 2). The basin's axis spreads over Wyoming and Montana with a NNW-SSE and NNE-SSW trend, respectively (De Bruin, 1993).

Major deformation in the basin started in the early Eocene and was probably active until the Miocene (Strickland, 1958). Thom and Spieker (1931) suggested that deep seated reverse faults and extensional fissures/openings on anticlinal surfaces were formed by the forces from west side, whereas an east–west trending normal fault was mapped by Wegemann (1911) that splits the Teapot Dome field into northern and southern portions. TSF and its equivalent Minnelusa Formation are the major producing Paleozoic reservoirs in PRB. The majority of petroleum accumulations in the PRB are trapped in stratigraphic units, or at few places, in anticlinal closures. In the TSF, hydrocarbons accumulations are mainly found in structural traps (Dolton and Fox, 1995).

The Permian Phosphoria Formation is the established source rock that expelled a huge amount of hydrocarbons which later became confined in the TSF and Minnelusa Formation of the PRB, as well as several Paleozoic reservoirs of the Rocky Mountains (Cheney and Sheldon, 1959; Sheldon, 1967; Friedmann et al., 2004; Anna, 2009). Alternative sources for the petroleum are suggested by Clayton and Ryder (1984). They proposed interbedded black shales of the Minnelusa Formation might have discharged the hydrocarbons into the Minnelusa reservoirs in the eastern portion of the basin. Other petroleum reservoirs include the Muddy sandstone, second Wall Creek member of Frontier Formation, and Carlie shale (Turner member) of the Cretaceous age. The major source rock for the Cretaceous reservoirs is Mowry shale (~12 billion barrels charged oil) with fewer contributions from the Niobrara and Carlie shales (Momper and Williams, 1984; Dolton and Fox, 1995).

In the study area, Precambrian basement underlies thin interbedded sandstone successions, limestones, dolomites and evaporites of Paleozoic age (Figure 3). TSF is one of the major producing reservoirs at theTeapot Dome. Paleozoic strata are overlain by the dominantly terrigenous beds of Triassic and Jurassic age. The Upper Jurassic Sundance Formation has yet not produced HC in the Teapot Dome, but it surely has the potential to produce because of HC production in the adjacent Salt Creek field. A range of fluvial to marine sandstones and shales (Cretaceous) are present at the Teapot Dome field. Both the Shannon sandstone member of Cody shale and the Second Wall Creek member of Frontier Formation are the major Cretaceous producers at the Teapot Dome. Members of the Niobrara shale, Steele shale (Upper Cretaceous), as well as sandstone members of Thermopolis shale, Muddy sandstone, and Dakota sandstone (Lower Cretaceous) are also producing hydrocarbons in the Teapot Dome field (Dennen et al., 2013).

Datasets and methodology

The datasets utilised in this study include poststack seismic sections and some well log records. A 28-square-mile 3D seismic cube of poststack seismic data is used in delineating the seismic structural elements and performing the seismic inversion analyses. Reservoir evaluation was done using the available well log records of 17 wells scattered within the study area. The subunits of TSF (A-sandstone, B-dolomite and B-sandstone) were identified from core data and well correlation (Schwartz, 2006; Jafri et al., 2016). Results were then integrated by applying fuzzy logic module in a GIS platform. The adopted methodology and integrated techniques is shown as a flowchart in Figure 4.

Well logging analyses

Standard well-logging procedures for areas with similar reservoir characteristics that are well known in the petroleum industry are used for evaluation of TSF and extracting the necessary petrophysical parameters for seismic data inversion (Morris and Biggs, 1967; Serra et al., 1984; Schlumberger, 1986, 1991; Abd El Rahman and Lashin, 2004; Asquith et al., 2004; El-Naby et al., 2009; Lashin et al., 2003, 2011, 2014; Lashin and El Din, 2013; Mohamed et al., 2013; Lashin and El-Naby, 2014; Jafri et al., 2016; Naeem et al., 2015).

Quantitative well log analysis was done to evaluate the identified subunits. Shale/clay volume was estimated for TSF using gamma ray log data (Larionov, 1969). Several frequency cross-plots were generated to determine necessary shale parameters (φN_{shale}, ρb_{shale}, Δt_{shale}, Rt_{shale}) that are required for reservoir characterisation (Schlumberger, 1991;

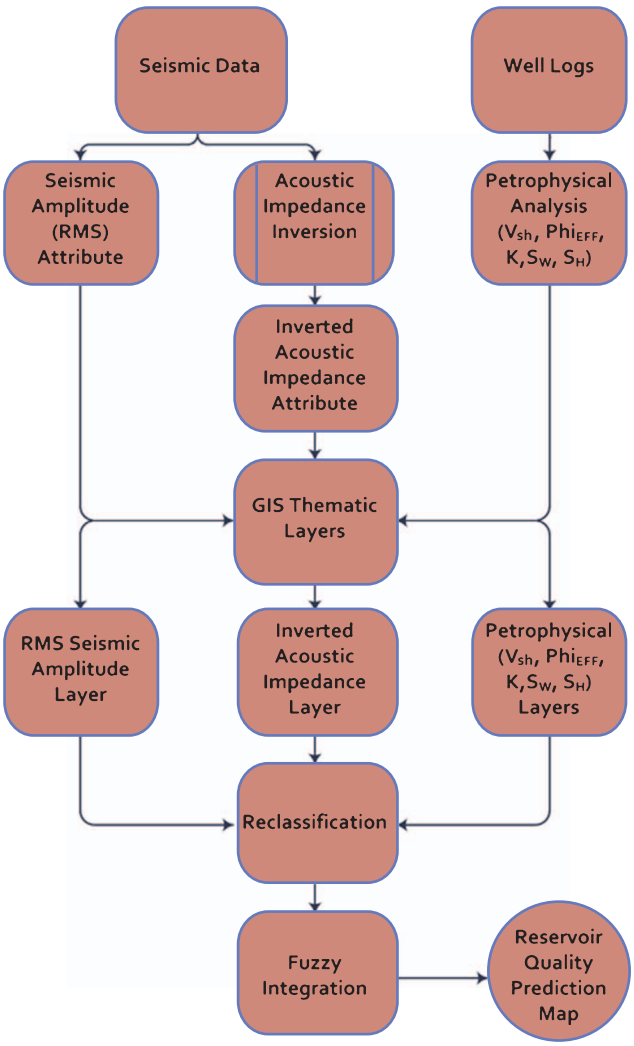

Fig. 4. Flow chart showing the formulation of research methodology.

Jafri et al., 2016; Lashin et al., 2016). Total porosity (ϕ_T) was calculated using a neutron-bulk density combination ($\phi_{N\text{-}D}$) and then further corrected for shale volume to give the effective porosity (ϕ_{Eff}). Formation water resistivity (R_w) was calculated by spontaneous potential and Picket plot methods (Serra et al., 1984; Schlumberger, 1986, 1991; Asquith et al., 2004). Subsequently, the Archie equation was used for water saturation (S_w) estimation from which hydrocarbon saturation (S_H) was calculated (Archie, 1942). Since the overlying and underlying units of the studied B-reservoir attain good carbonate lithology, a mixed petrophysical model (Saraband and Coriband) is selected and applied in logging analyses. The

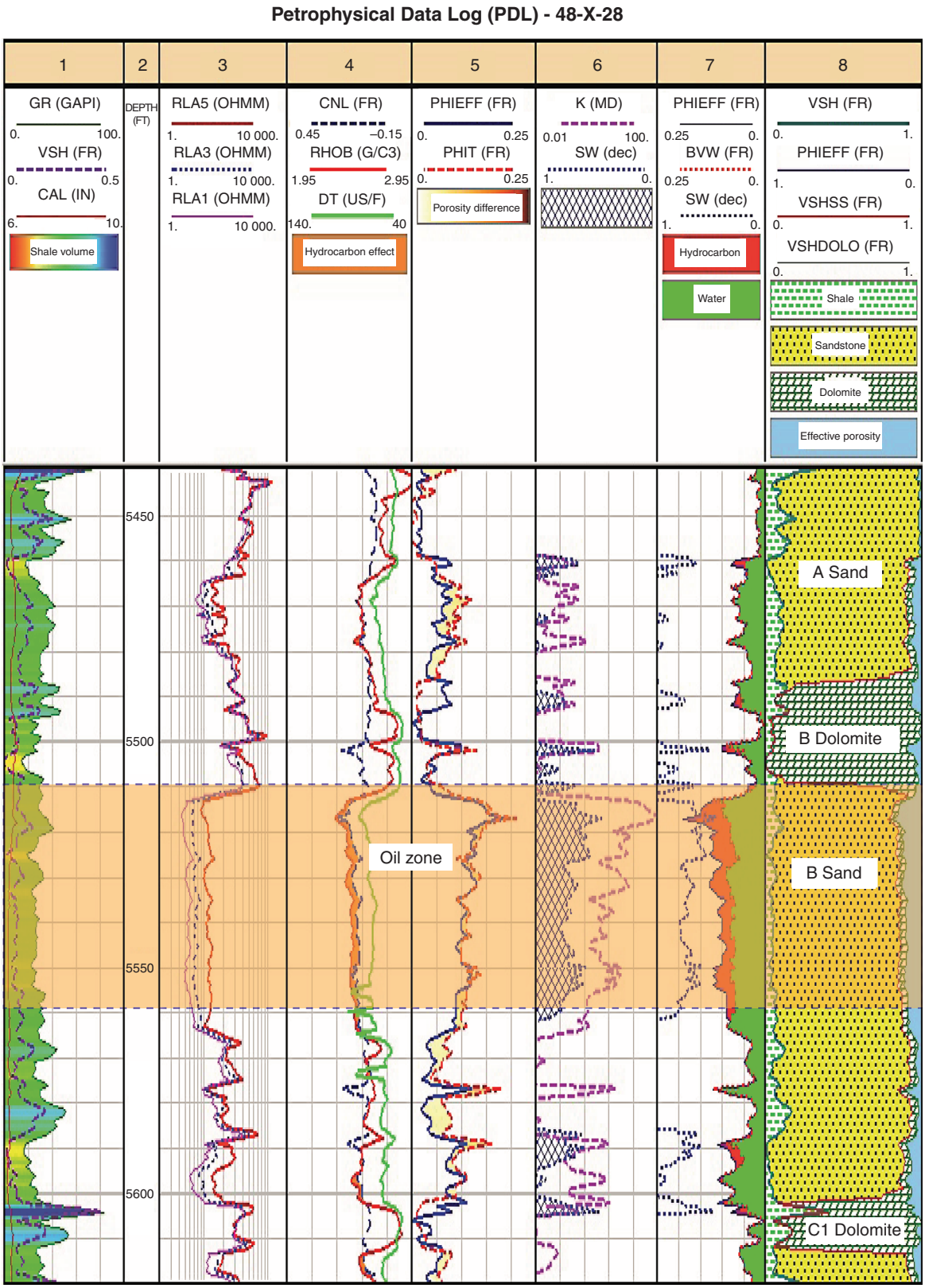

Fig. 5. Petrophysical data log of B-sandstone reservoir, well 48-X-28.

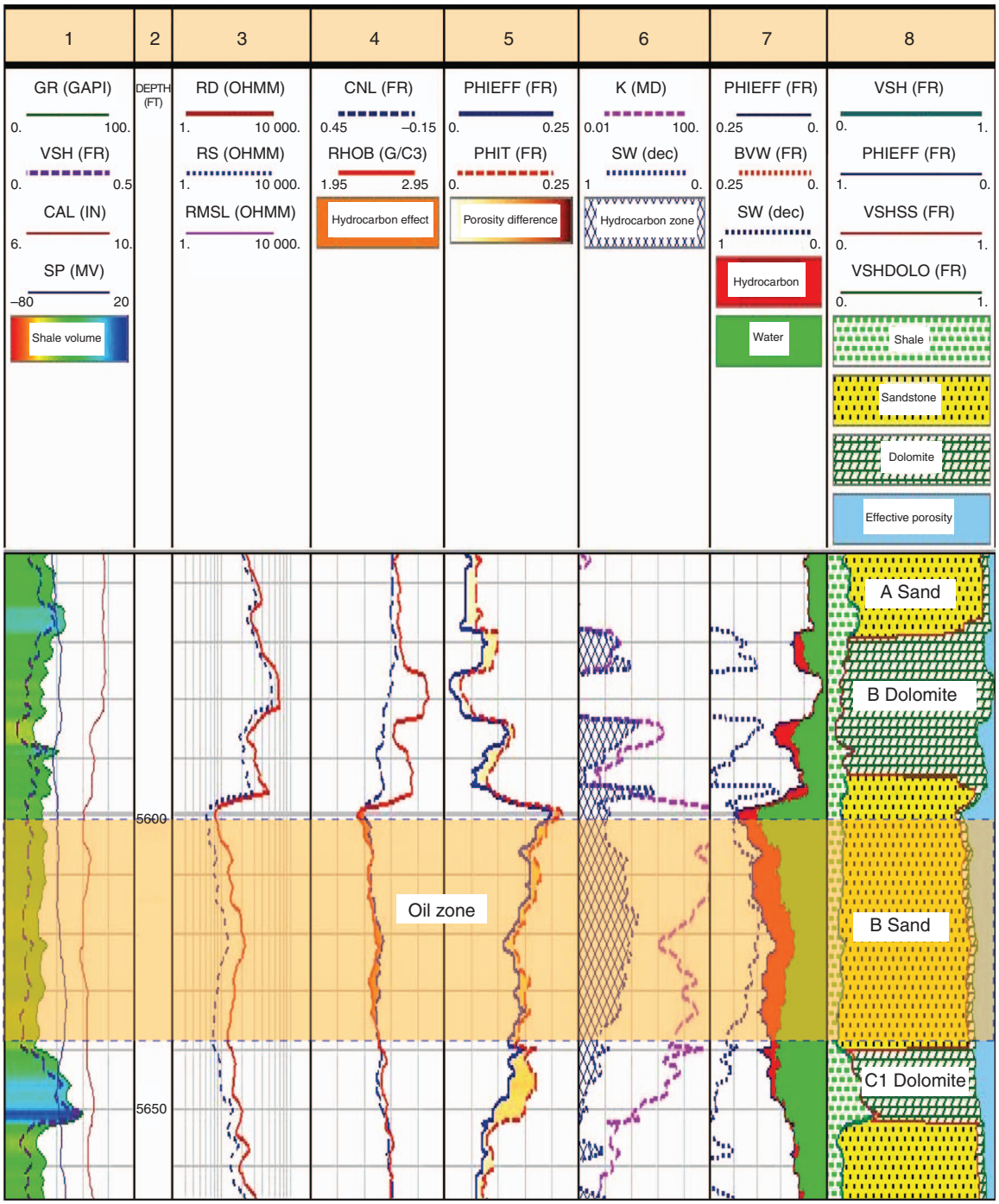

Fig. 6. Petrophysical data log of B-sandstone reservoir, well 51-CMX-10-WD.

Saraband model is applied for the sandstone zones, while the Coriband model is applied for the carbonate lithology (Schlumberger, 1986, 1995).

The most important reservoir properties are displayed in several vertical analogues (Figures 5 and 6) and fluid distribution maps (water and hydrocarbon, see Figure 7) to check for the spatial variation of the reservoir characteristics, both vertically and laterally.

Seismic data analysis

The 3D poststack seismic data cube is used mainly to enhance the seismic structural and inversion analyses in the study area (Figure 8). Faults and horizons above and below the TSF were interpreted, and the two-way time (TWT) structure mapping was done on top of the TSF. Synthetic seismograms (SSs) were generated for the well-to-seismic tie and to pick the horizon on the seismic data. Check shot data were also available to calibrate the well data with seismic data. The PSAI inversion approach was adopted to delineate the reservoir properties using Hampson Russell software (Duijndam, 1988; Latimer et al., 2000; Ulrych et al., 2001; Russell and Hampson, 2006).

Seismic structural analysis

A comprehensive seismic structural analysis, including picking and interpretation of horizons, detecting the subsurface structures and detecting the entrapment of the encountered hydrocarbons is achieved. In addition, a time-depth-velocity

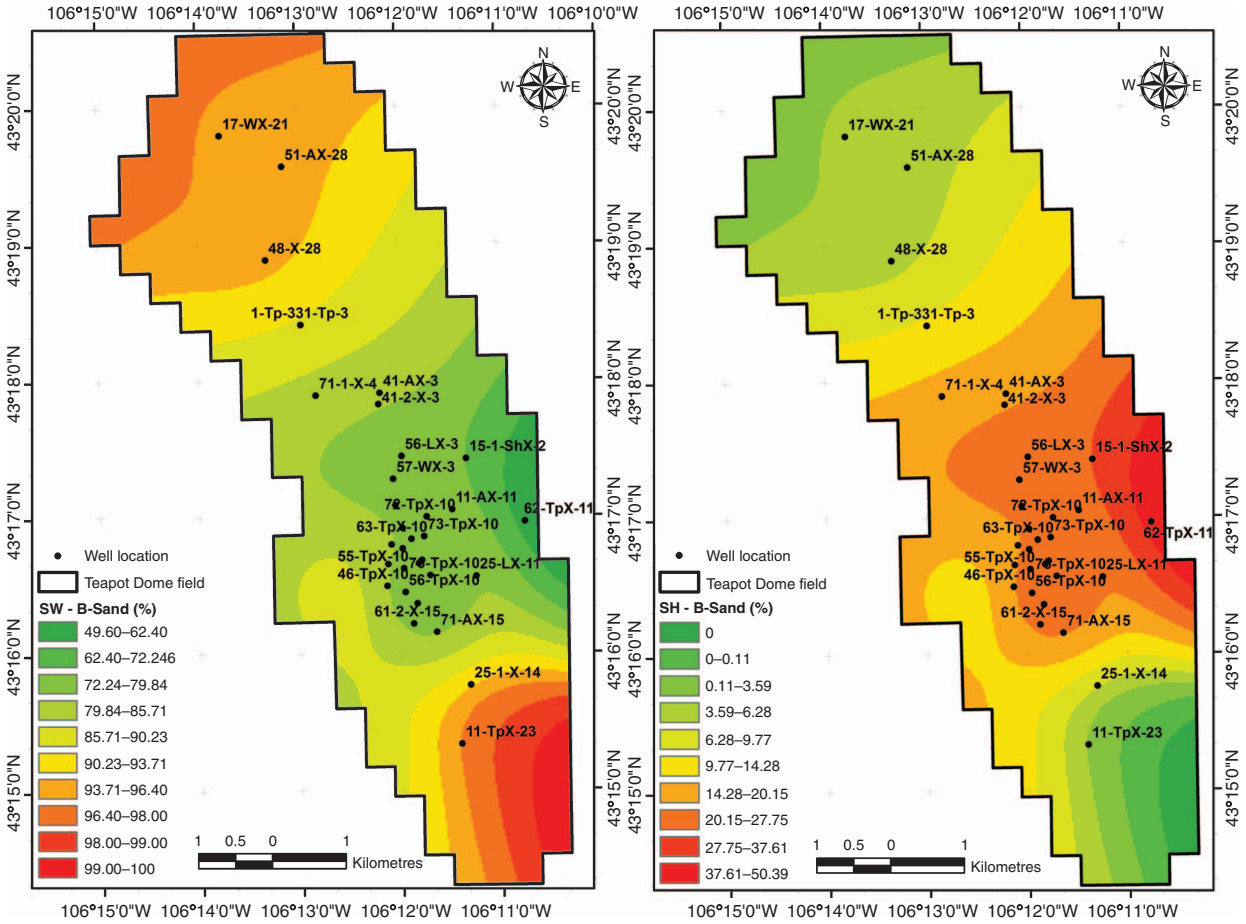

Fig. 7. Water and hydrocarbon saturation maps of B-sandstone reservoir.

analysis is executed and several TWT structural, depth and velocity maps are constructed for the top of the main oil-bearing reservoir (TSF).

Synthetic seismograms and well-to-seismic tie

Several synthetic seismograms (SSs) are constructed to perform well-to-seismic tie and identify the seismic horizons. Sonic and density log, plus an extracted source wavelet, were used to construct the SSs. Petrel software was used for the synthetic seismogram construction, and the wavelet was extracted from the seismic data by the Extended White method (Walden and White, 1998) because of its greater viability with our dataset compared to the statistical synthetic wavelet. Mathematically, it can be expressed as:

$$s(t) = w(t) \times r(t) + n(t)$$

where $s(t)$ is the convolutional model of the seismic trace, $w(t)$ is source wavelet, $r(t)$ is reflectivity series and n is noise (for more details see Walden and White, 1998).

Eight wells were selected for SSs generation based on the availability of sonic and density logs. To produce the SSs and reach a best match between derived and real seismic data, a statistical wavelet was extracted and then convolved with the well driven reflectivity series. Well-to-seismic tie was done to accurately identify the reflection events on the seismic data (Figure 9). The eight selected wells were correlated with the 3D seismic cube within a radius of 110 ft. Correlation between the well and seismic data was more than 95% in all the wells, which is suitable enough to use these wells for seismic inversion.

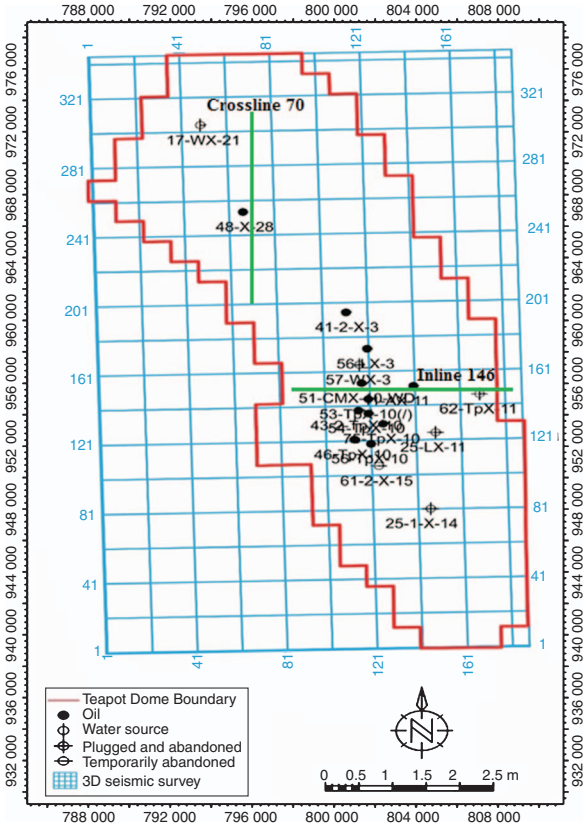

Fig. 8. Seismic base map of study area.

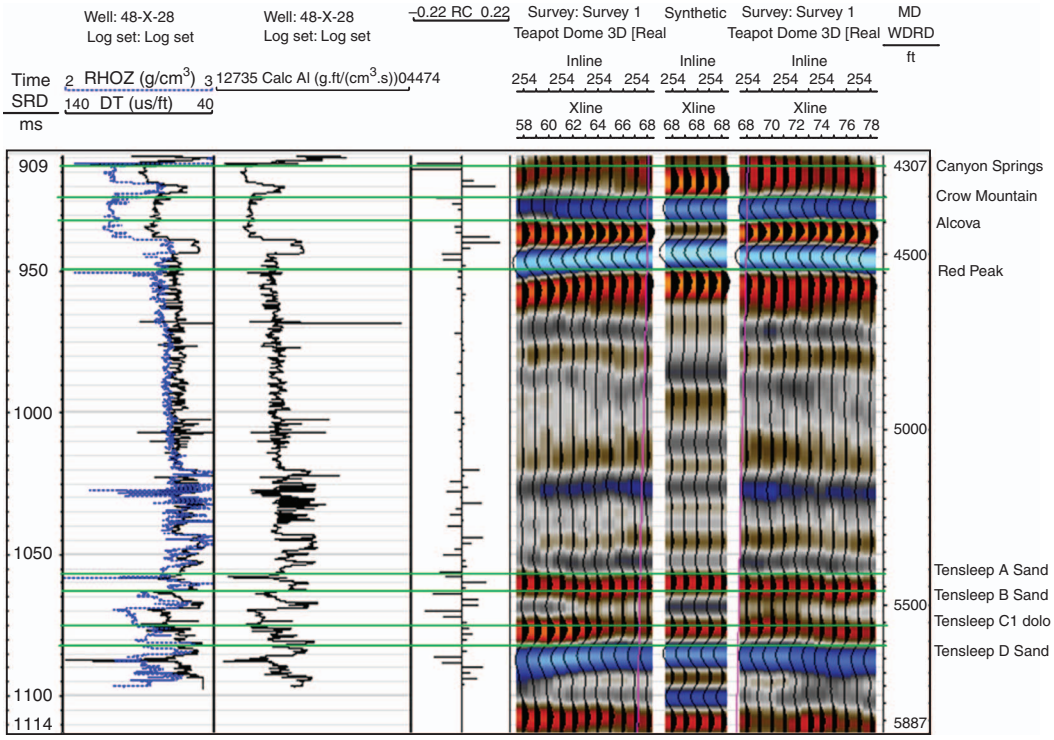

Fig. 9. Log-derived synthetic seismic trace as matched with the actual seismic trace.

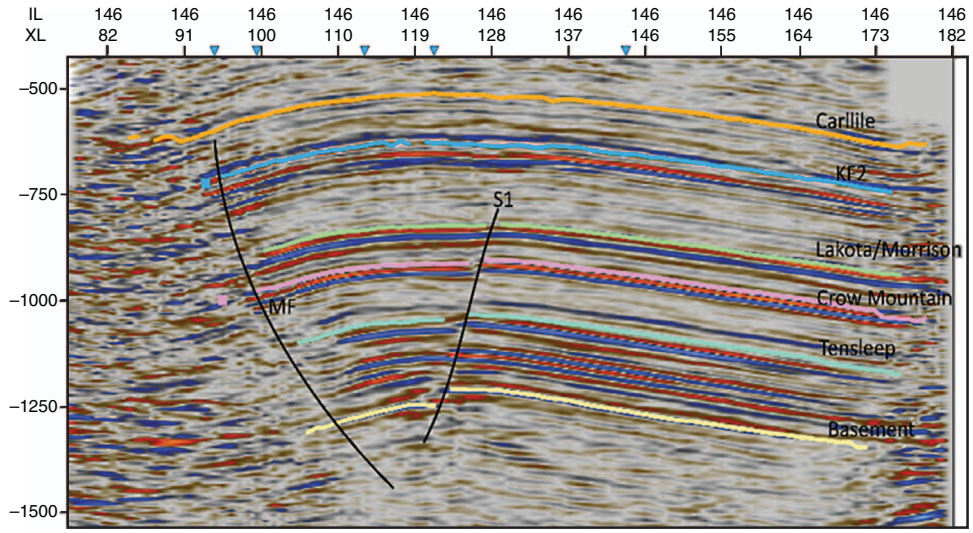

Fig. 10. 2D interpreted seismic section (inline 146) passing through the study area.

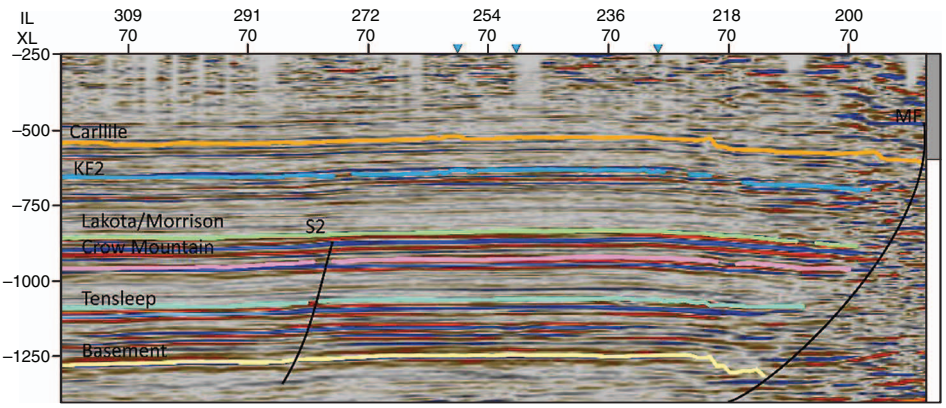

Fig. 11. 2D interpreted seismic section (crossline 70) passing through the study area.

Velocity analysis and horizons picking

Once the SSs are constructed, they are correlated with real seismic data in order to decide the best horizons for further interpretation. Analysis of the traveltimes (one- and two-way) and velocity records with depth (average and interval) are enhanced in conjunction with the interpretation of the SSs to help identify different rock unit boundaries. Horizon picking and interpretation was done on the basis of the SS signature matching with real seismic data using the complete 3D seismic survey to delineate the aerial distribution of different stratigraphic horizons in the area. The main objective of the horizon picking was to render the top of the TSF as well as the overlying horizons. Several two-dimensional (2D) interpreted seismic and 3D visualisation sections are constructed (Figures 10–12). TWT structural, depth and velocity maps are generated at the top of the Tensleep Formation (Figures 13 and 14).

PSAI analysis

The PSAI technique was first introduced in the beginning of 1980 (Lindseth, 1979). It produces results with much higher resolution and enhanced interpretation than other techniques,

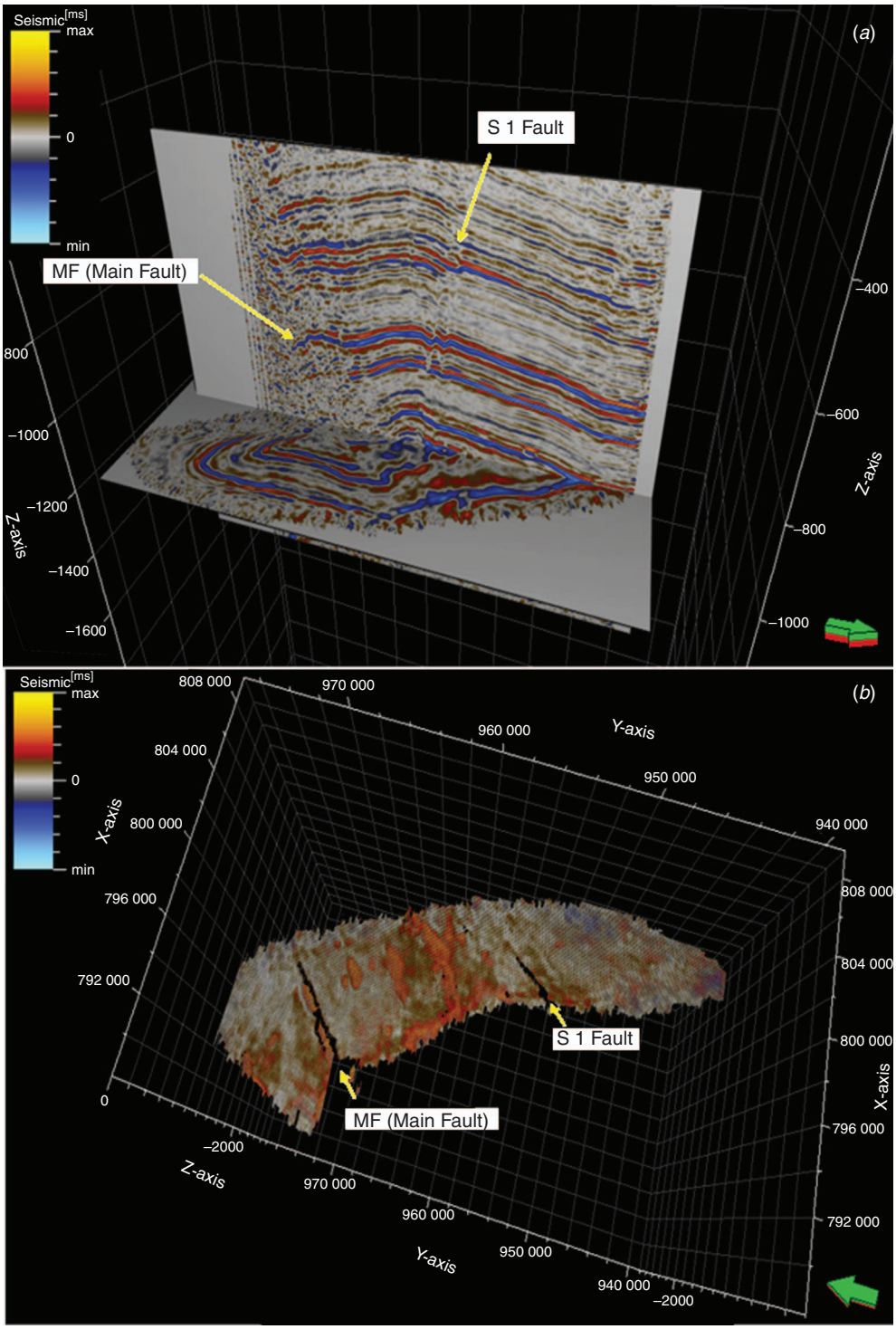

Fig. 12. (*a*) 3D seismic sectional view and (*b*) SA surface for crossline 100 at a time slice of 1248 ms.

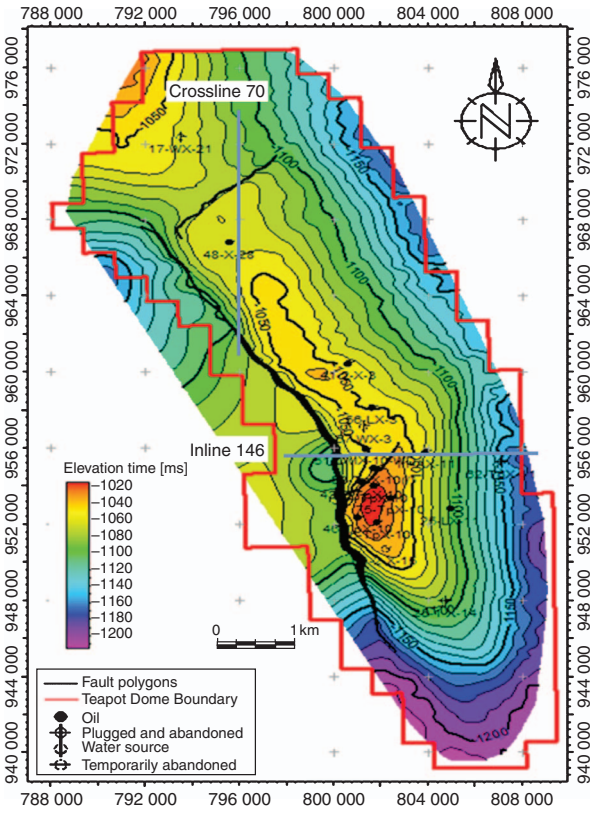

Fig. 13. TWT structure map at the top of Tensleep B-sandstone reservoir.

and can therefore reduce drilling risks (Pendrel, 2001). This approach is usually carried out on the reservoir level to precisely delineate its properties (Duijndam, 1988; Ulrych et al., 2001; Latimer et al., 2000; Shrestha and Boeckmann, 2002; Pendrel, 2006).

AI inversion is a process in which an pseudo-acoustic impedance log is generated at every seismic trace to construct a geological model/framework of the subsurface. It converts the surface seismic data to distinct blocky-layered characteristics that directly correspond to the subsurface geological model. As mentioned before, density and sonic logs are used, and a specific type of wavelet is extracted, to generate SSs and then reach a best match between derived and real seismic data (see *Synthetic seismograms and well-to-seismic tie*, under *Seismic structural analysis*). The PSAI approach is carried out on the reservoir level to delineate its reservoir properties. Brown (2004) defines six types of poststack inversion techniques. In the present work, the AI inversion (blocky) technique is adopted. The adopted approach includes the construction of a background low frequency (initial) model from seismic and well logs data to see the impedance distribution of the subsurface geological model.

Initial impedance model (low frequency)

Initial impedance or low frequency model (LFM) is of critical importance in seismic inversion process because it restores the low frequency content in the data. LFM broadens the amplitude spectra and adds a low frequency component to the recorded seismic data, hence improving the resolution/quality

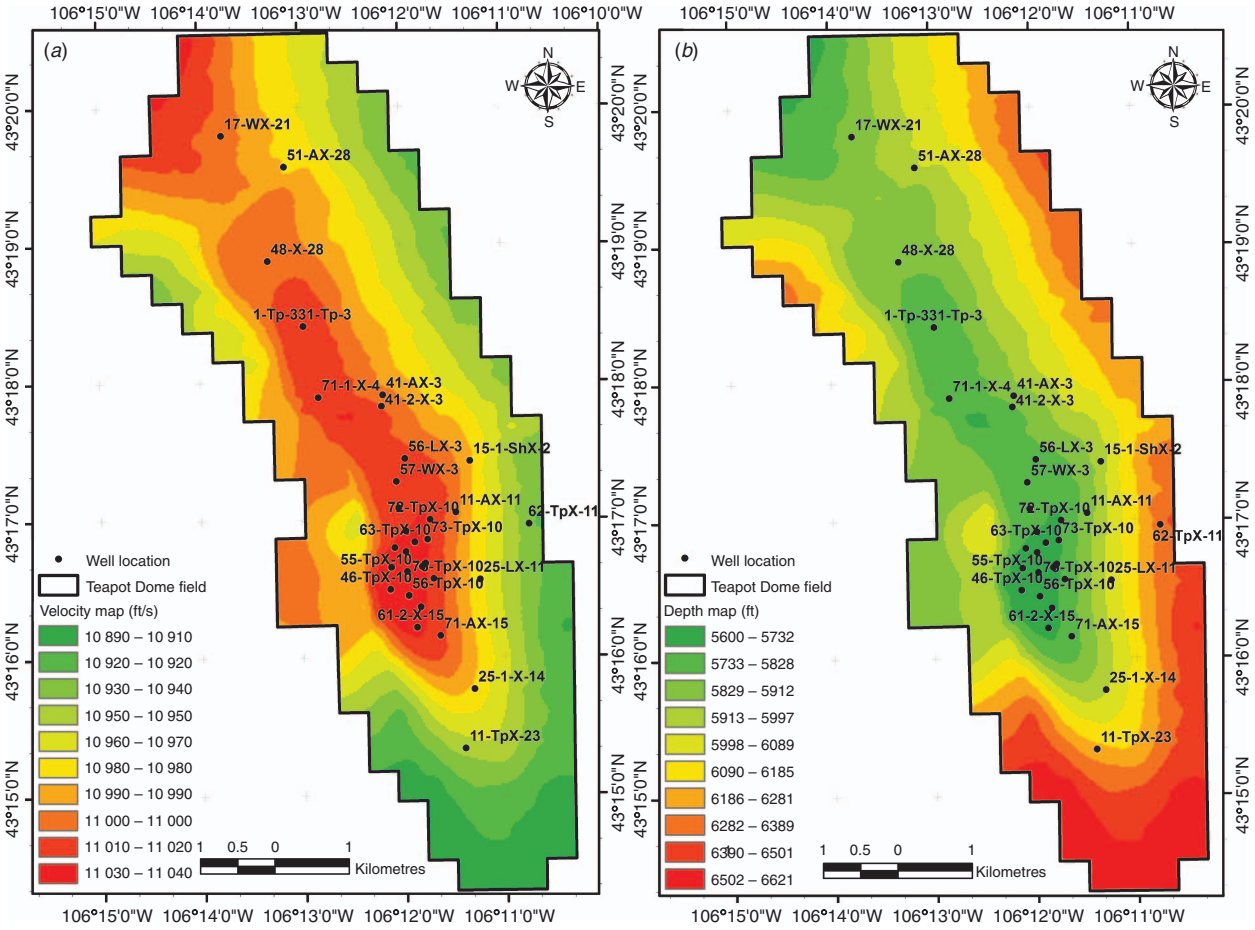

Fig. 14. (*a*) Velocity distribution map and (*b*) depth conversion map at the top of Tensleep B-sandstone reservoir.

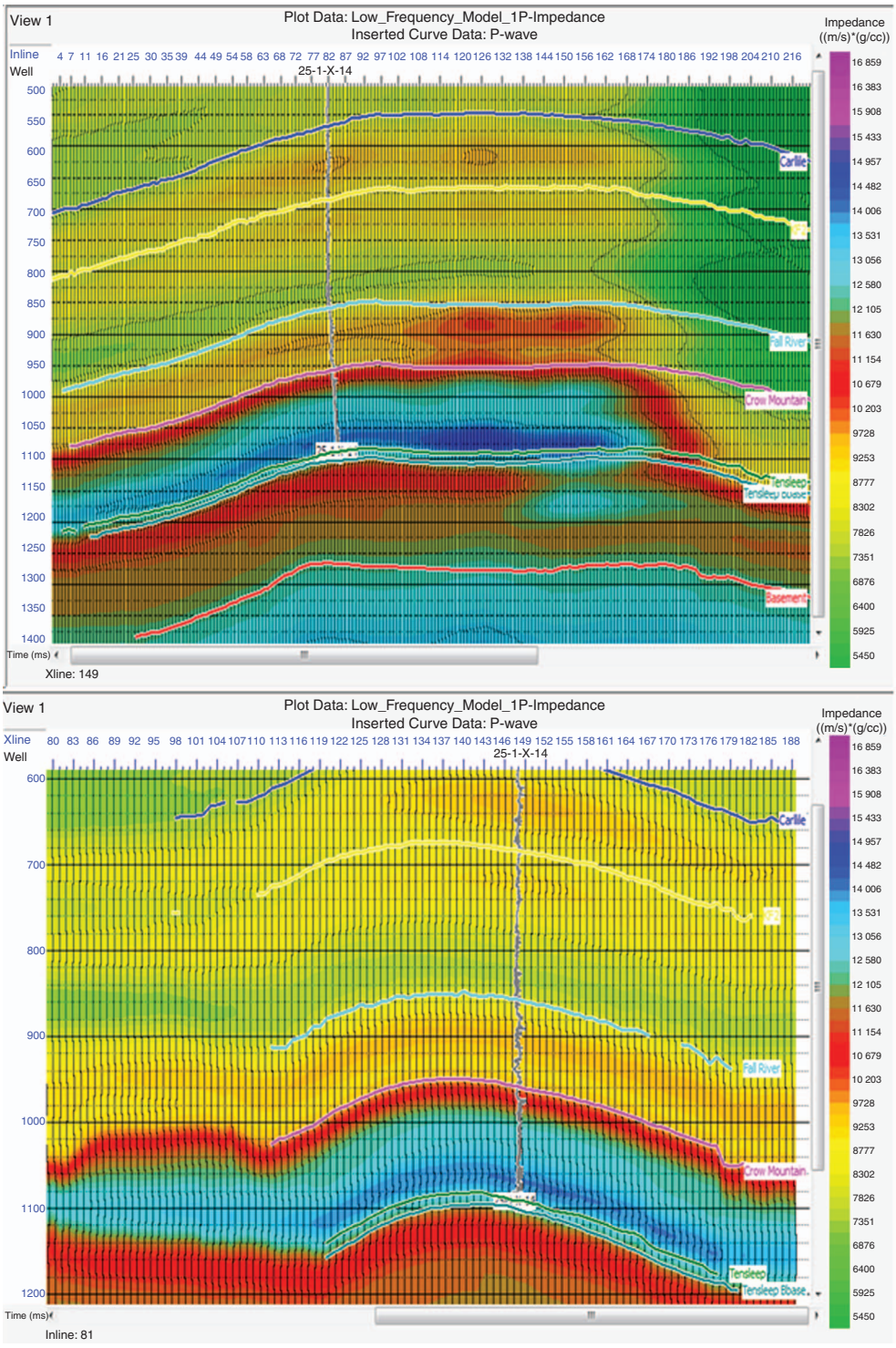

Fig. 15. Two generated low frequency cross-sections (inline 81 and crossline 149) passing through well 25–1-X-14.

of the data, which leads to a good reservoir characterisation (Chambers and Yarus, 2002; Chopra and Marfurt, 2006; Lloyd and Margrave, 2011; Naeem et al., 2015). Sonic-density logs are used and the different horizons are picked and interpreted to provide the lateral constraint within the 3D seismic cube. Eight wells were used for the estimation of LFM. A time window of 500–1500 ms was used for the LFM estimation and a high cut frequency filter of 10–15 Hz was applied (Figures 15 and 16).

GIS thematic layers

Applying fuzzy logic in an ArcGIS platform has two main steps: fuzzification/reclassifying and the overlay analysis. The transformation of the actual input attribute values to the possibility scale of membership (here 1–5) is termed as process of fuzzification (Esri, 2011). Fuzzification can be explained by an example: if in a predictive model of reservoir quality, permeability is an input attributed to a predictive reservoir

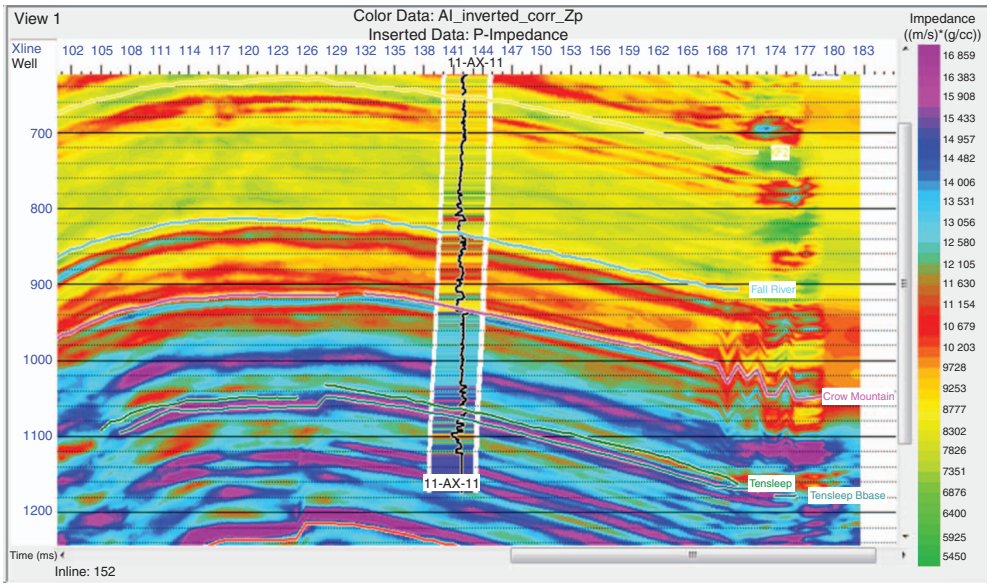

Fig. 16. Inverted AI section along crossline 152 passing through well 11-AX-11. AI derived from well data is overlaid along the well trajectory.

quality, then every permeability value should be assigned a value between a scale range (here 1–5) that pertains to the suitability of that permeability class towards the reservoir quality. The magnitude of value '5' defines the maximum certainty in the set with maximum suitability, whereas the value of 1 is indicative of the value in the set with minimum certainty. The values in the transition between 1 and 5 represent some possibility, with higher values indicating more membership likelihood (Esri, 2011).

Results from the petrophysical evaluation and seismic inversion are then integrated using fuzzy logic AND operator in order to identify the TSF subunit with better reservoir quality and hydrocarbon potential in the study area. Six thematic layers i.e. shale volume, effective porosity, permeability, water saturation, inverted AI and seismic amplitude (SA) were prepared using ArcGIS 10.2 software. The first four layers are based on the well log analysis and prepared on the top of B-sandstone unit (Jafri et al., 2016). The last two layers were derived from the seismic inversion analysis and averaged in time over the B-sandstone unit. A fuzzy prediction map is then generated where the best reservoir area is indicated.

Results and discussion

TSF reservoir properties

The detailed well log analysis and the main reservoir properties of the TSF are gathered and presented in several vertical analogues and fluid distribution maps (Figures 5–7). Two vertical analogues are selected as examples (Figures 5 and 6 for wells 48-X-28 and 51-CMX-10-WD) to demonstrate the vertical distribution of hydrocarbon potential and B-sandstone reservoir properties.

Petrophysical data log of well 48-X-28

Well 48-X-28 lies in the northern part of the Teapot Dome field (see Figure 1 for location). One hydrocarbon-bearing zone is clearly observed at the upper part of the B-sandstone unit at a depth interval of 5511–5562 ft (Figure 5). It exhibits good reservoir properties and hydrocarbon signatures in terms of low shale volume (gamma ray range of 20–35 API giving rise to V_{sh} of 5%), good average effective porosity (> 12%), good permeability (> 50 mD) and considerable hydrocarbon content (up to 30%). Resistivity curves track away from each other causing a prominent separation among them. Deep resistivity reads up to 60 Ω m. Effective porosity is 18% at the top, which decreases with depth down to 10%.

Petrophysical data log of well 51-CMX-10-WD

This well lies in the centre of the Teapot Dome field (see Figure 1 for location). One zone is identified in the B-sandstone unit at 5599–5638 ft depth interval. This is a thick zone with low GR intensity (20–30 API) and low shale volume. Effective porosity varies between 19% in the upper part of the zone and 11% in the lower part of the zone. Hydrocarbon saturation is in the range of 40–50%, and the zone's permeability is very good from 30 mD to more than 100 mD. Some hydrocarbons are indicated at the overlying dolomite unit (Figure 6).

Based on such analysis, the B-sandstone zone was identified to have the best reservoir characteristics, with an effective porosity range of 5–20%, permeability 0.1–250 mD and hydrocarbon saturation up to 72% (Jafri et al., 2016). Hydrocarbon saturation increases remarkably at the middle part of the field and tends to decrease towards the northern and southern portions (Figure 7). The other important petrophysical parameters (V_{sh}, ϕ_{Eff}, and K) of the B-sandstone reservoir are generated as GIS thematic layers and interpreted with the seismic inversion parameters.

Interpretation of seismic data

Structural framework

Figure 9 shows an example of the constructed SSs regarding 48-X-28 well. Seismic data are extracted within 110 ft distance on either side of each well and compared with synthetic and seismic ones. It shows the generated AI and the final matched synthetic trace, as tied with the actual seismic trace of inline seismic section 254.

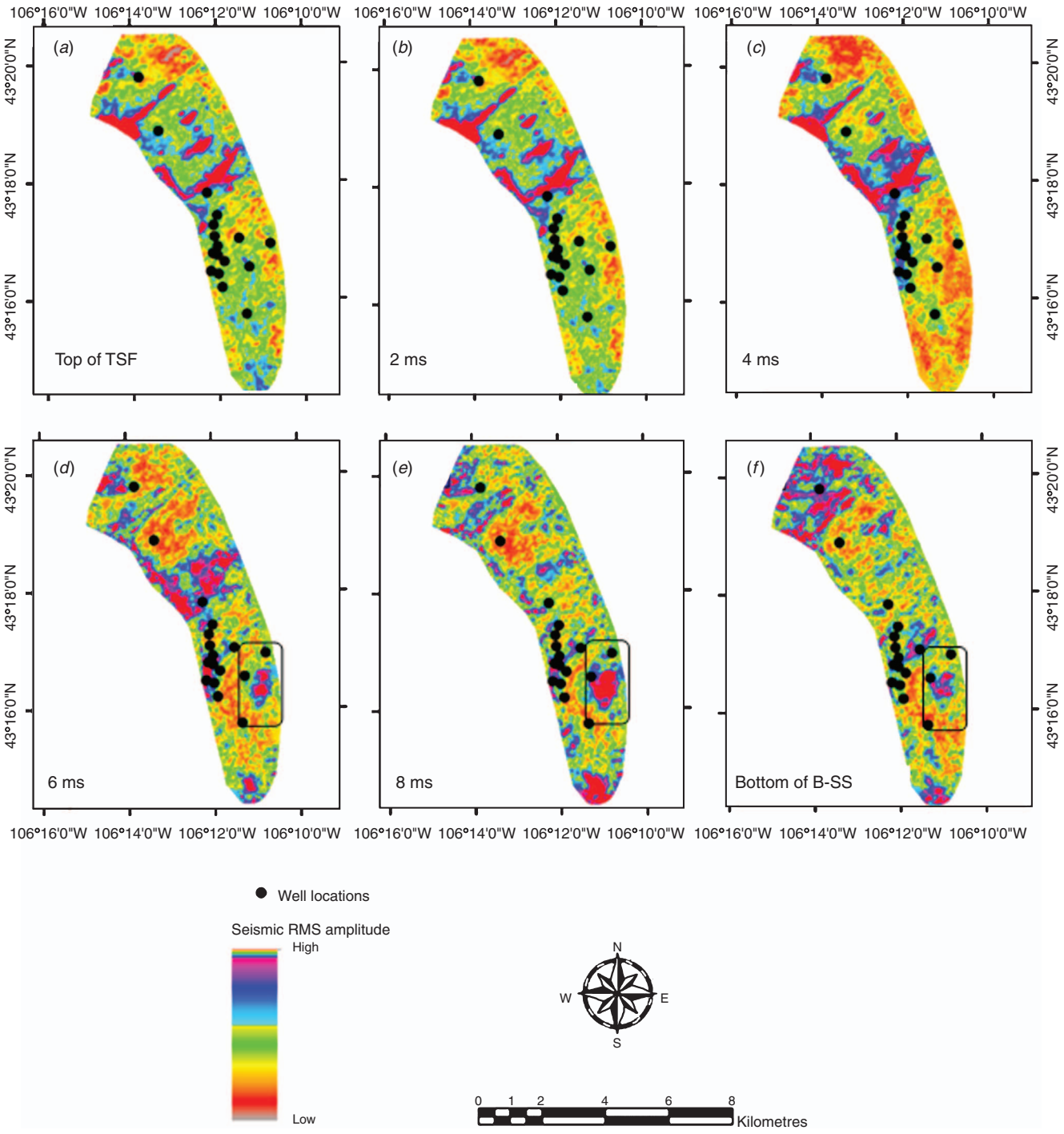

Fig. 17. SA (RMS) slices: (*a*) at top of Tensleep Formation, and (*b–f*) below Tensleep with an increment of 2 ms each. The rectangular portion in (*d–f*) represents the prospective zone for future exploitation.

Tops of the main formations are detected and displayed. The top of TSF is detected at a TWT of 1.065 s.

Several 2D seismic sections are constructed and interpreted. Figures 10 and 11 show two interpreted inline and crossline seismic sections, selected as examples (inline 146 and crossline 70, see location at Figure 8). The different picked horizons seem to be flat through the course of the study area. A major reverse fault (MF) trending NNW–SSE was interpreted at the western margin of the field, providing a fault bounded closure to the anticline. Two more perpendicular low dipping normal faults (S1 and S2) were interpreted having normal sense of movement and trending roughly east–west (see TWT map, Figure 14). The interpreted fault pattern is in agreement with the general geological setting of the area and the prevailing structural elements (Thom and Spieker, 1931; Strickland, 1958; De Bruin, 1993).

3D visualisation was done to better illustrate the structural features at the Teapot Dome field. Figure 12*a*, *b* shows a 3D sectional view for crossline 100 and at a time slice of 1248 ms. The displacements of the main thrust fault and the splay normal fault can be clearly seen on the 3D seismic section (Figure 12*a*) and as a discontinuity in the signals of the SA surface (Figure 12*b*).

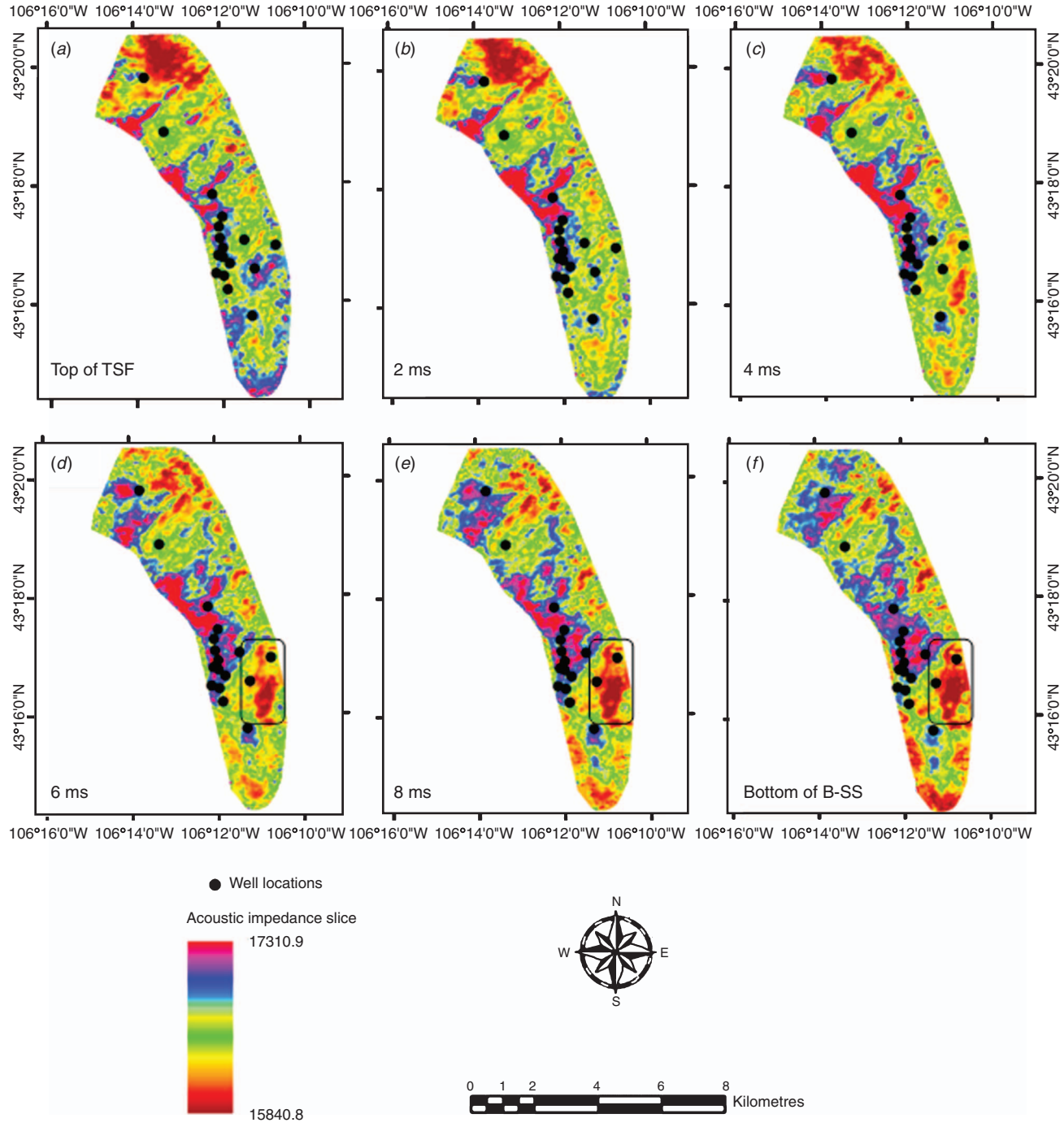

Fig. 18. Inverted AI slices: (*a*) at top of Tensleep Formation, and (*b–f*) below Tensleep with an increment of 2 ms each. The rectangular portion in (*d–f*) represents the prospective zone for future exploitation.

Time structural, velocity and depth maps

Only one TWT structure map is generated for the main oil-bearing reservoir in the study area (Tensleep B zone). The map shows the structural trends, fault orientation, and the domal/fault bounded structural highs, which could act as possible structural traps in the area (Figure 13). It shows that the structure at Tensleep is an anticlinal one, bounded by a major reverse fault at its western margin. The Tensleep anticlinal structure is trending NW–SE, and the major fault has the same trend and offsets as the Precambrian basement (Friedmann and Stamp, 2006). It is a doubly plunging anticline that seems to be the key factor controlling the entrapment of Tensleep reservoirs at the Teapot Dome. The asymmetrical nature of the anticline is very prominent with its gently dipping eastern limb and the steeper western limb.

The velocity and depth maps confirm the dominant domal structure in the study area (Figure 14*a*, *b*). The average velocity map shows a remarkable NW–SE increase in the middle of the study area associated with a similar trend of decreasing depth (5600–7532 ft). A maximum velocity (11010–11040 ft/s) record is indicated at the middle axial area of the structure (apex of the anticline) where wells 75-TpX-11 and 76-TpX-10 are located. The main hydrocarbon potentiality is detected in this area with a remarkable eastward increase (see HS map, Figure 7*b*).

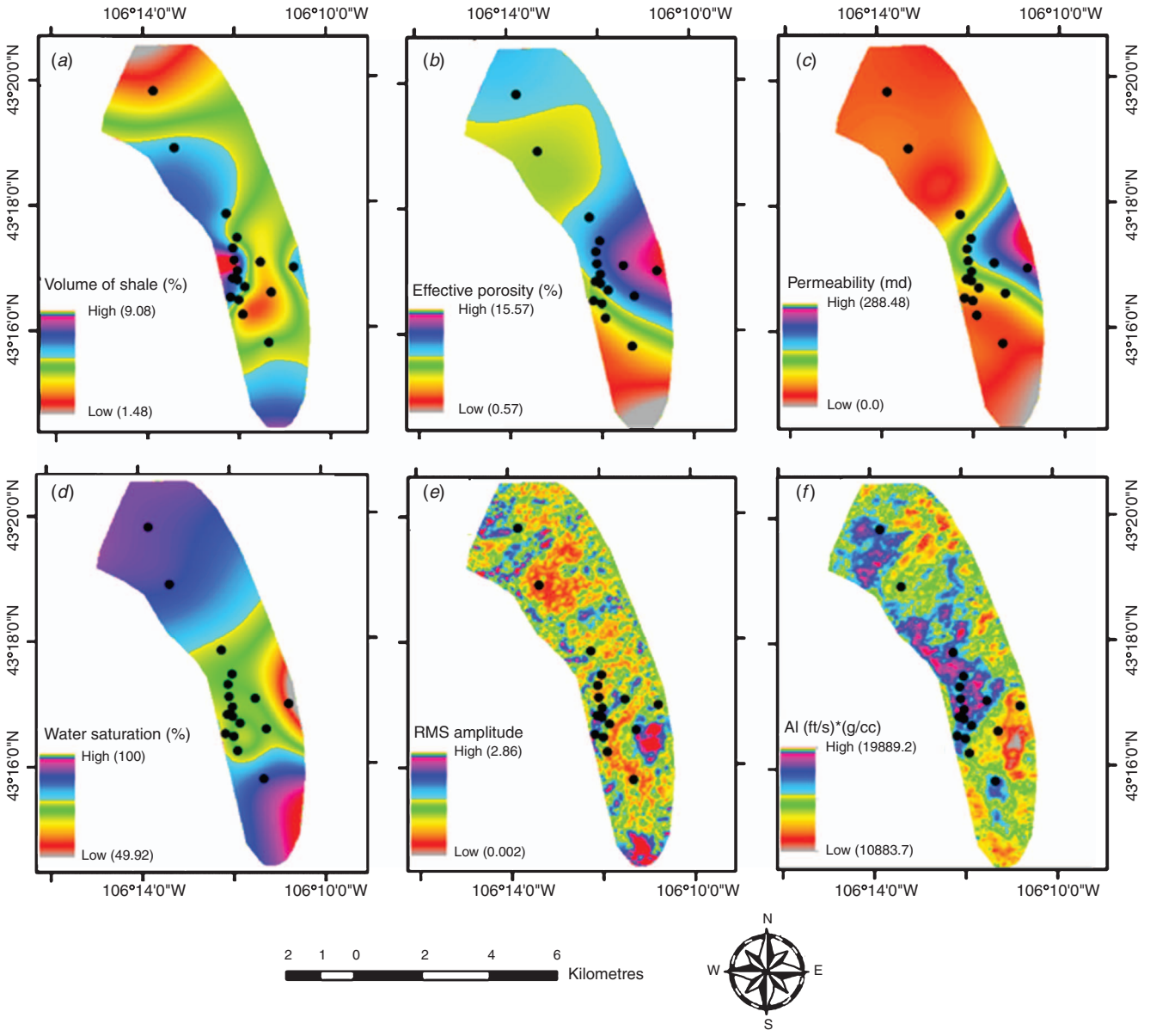

Fig. 19. GIS thematic layers constructed on top of the B-sandstone unit showing the lateral distribution of the respective reservoir parameters in the field: (*a*) Volume of shale, (*b*) effective porosity, (*c*) permeability, (*d*) water saturation, (*e*) seismic RMS amplitude attribute, and (*f*) inverted AI attribute.

Poststack seismic inversion results

The derived synthetic seismic data at respective well locations are compared with the actual surface seismic data. The degree of matching between the two seismic datasets is measured by means of cross-correlation. Good correlation is reached between the synthetic seismic traces and actual seismic sections, indicating that the parameters used for inversion analysis were appropriate and could be further used in inverting the whole seismic volume of the Teapot Dome (see *Synthetic seismograms and well-to-seismic tie*, under *Seismic structural analysis*).

LFM sections

Figure 15*a*, *b* shows two generated low frequency cross-sections (inline and crossline) passing through well 25–1-X-14. They display the P-impedance along the well trajectory and the interpreted horizons. Well-to-seismic correlations greater than 97% are selected to estimate the initial LFM within the survey limits. Considering the aim of the study 'to delineate the reservoir characteristics', a time window of 500–1500 ms was selected for the initial impedance model estimation, which also surrounds the top and bottom portions of the reservoir. A high cut frequency filter (10–15 Hz) was applied to get the low frequency content only. Figure 16, on the other hand, shows the initial impedance model passing through well 25–1-X-14. P-wave AI along the respective well path and the interpreted horizons within the selected time window are also displayed in the section. The different horizons are clearly differentiated in terms of their inverted AI values, and a colour code is defined for each zone (see colour legend to the right of the section).

SA and AI slices

In order to better understand the reservoir characteristics of our target level, AI and root mean square (RMS) seismic raw amplitude slices are extracted at the top of reservoir of Tensleep Formation. A total of six slices were extracted with

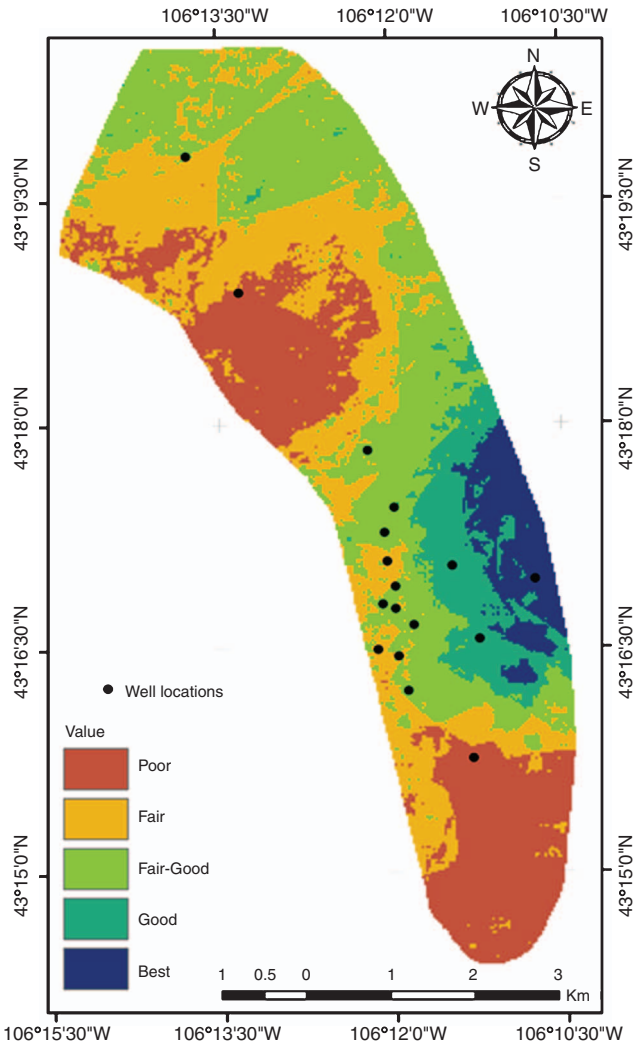

Fig. 20. Reservoir quality prediction map produced by integrating the six layers using fuzzy logic.

an increment of 2 ms up to 10 ms below the Tensleep Formation. The SA and inverted AI slices are extracted at the top and just below the Tensleep Formation in the study area (Figures 17 and 18). It was observed that the RMS amplitude at the Tensleep reservoir level varies from its top to the bottom. More specifically, the amplitude is low at the selected zone at the top of Tensleep sandstone and tends to increase downwards with each 2 ms time increment. A prospective hydrocarbon-bearing high amplitude zone (highlighted in the Figure 17*d–f*) was identified based on the increase of seismic RMS amplitude.

It can be interpreted from the extracted slices that AI values are high at the top of Tensleep, but tend to decrease down to the depth of the reservoir (Figure 18*d–f*). The decrease in the AI value indicates that the selected zone attains good reservoir characteristics in terms of high hydrocarbon content.

The zone marked by the low AI and high seismic RMS amplitude corresponds to the B-sandstone unit, which was evaluated to have a porosity range higher than the upper two units (A-sandstone and B-dolomite, see petrophysical analogues Figures 5 and 6).

GIS thematic layering

The B-sandstone unit was declared as the major prospective reservoir unit among the three studied subunits of TSF (Jafri et al., 2016). The most important properties of B-sandstone reservoir, along with the seismic inversion parameters, are integrated in several thematic layers. These layers are classified into five equal interval classes using assigned fuzzy rating scale of 1–5. The value 5 indicates the highest contribution of the class towards the final reservoir quality prediction map and 1 indicates the least. It is important to emphasise that the classification/rating of the each individual layer was totally based on the common understanding and characteristics of the studied reservoir (i.e. main petrophysical properties and seismic inverted parameters).

By integrating the different layers, and selecting the best quality reservoir characteristics, we identified the rectangular marked area in Figure 19 as the optimum choice for a potential hydrocarbon reservoir. This area is characterised by relatively high RMS seismic velocity, low AI, low shale volume, high effective porosity distributions, as well as high hydrocarbon content compared to the rest of the area. TWT structural and depth maps clarify that this zone is lying on the limb of the major Teapot Dome anticline (see, Figures 13 and 14). Based on the petrophysical evaluation of the reservoir and seismic inversion analysis, a fuzzy prediction map (reservoir quality map) was generated (Figure 20). It clarifies the area of best reservoir quality that can be further recommended for future hydrocarbon exploitation.

Conclusion

An integrated approach was used to characterise the TSF subunits based on their potential for hydrocarbon production. The major lithology of the TSF is sandstone (quartz) and dolomite, with minor anhydrite and gypsum minerals. The B-sandstone unit was declared the best unit for hydrocarbon production based on the detailed petrophysical analyses results: an effective porosity range of 5–20%, permeability of 0.1–250 mD and hydrocarbon saturation up to 72%. The highest hydrocarbon potential is concentrated in the middle part of the field and tends to decrease towards the northern and southern parts.

A PSAI inversion (model-based) algorithm was applied to the 3D seismic data and an inverted AI cube was constructed. The inverted AI trace for every individual well was convolved with its respective extracted wavelet for SS generation. Seismic traces extracted in the vicinity of wells were used to calculate the cross-correlation of surface seismic and the inversion predicted response. The resulting cross-correlation was of higher degree, so the inversion results were concluded to be of suitable reliability. Full volume inversion was applied to a window of 500–1500 ms using the calculated parameters to get the inverted AI volume.

SA and inverted AI slices are extracted in a 10 ms window from the top of B-sandstone unit. A zone was identified on the SA slice, which marked a high amplitude anomaly that could be associated with good quality sands. The same zone was identified on the inverted AI slice with low AI values.

Reservoir characterisation using traditional/conventional techniques, based on well logs or laboratory measurements, tries to minimise or ignore the error that may arise due to uncertainty and fragile correlations between various datasets. In many cases it is difficult to relate a log response to a physical parameter due to several perturbing effects such as mineralogy, fluid types, shale content/types, etc.

Recently, fuzzy logic has been most commonly applied in formation evaluation and reservoir characterisation. It does not require normal distributions as commonly utilised in the

mathematically described conventional techniques. When dealing with a complex system using fuzzy logic, it is simpler to find a model of the parameters that drive and control the system, rather than finding a model for the system itself (Zadeh, 1965).

The advantage of utilising fuzzy logic is that it assigns probability (grayness) to the quality of the prediction on each petrophysical parameter of the reservoir. It asserts that there is useful information in this error (Norland, 1996; Cuddy, 1997). The error information can be used to provide a powerful predictive tool for the interpreter to complement conventional techniques.

Among the common three operators (AND, OR, NOT), the AND operator (min; x, y) is used, which is triangular norms with both operand and the result in (0, 1). This operator is selected based on its characteristics (commutative, associative, has 1 as an identity and increasing in each variable) and suitability for integrating all datasets a final perdition map.

The most important reservoir properties and seismic inversion results are incorporated together in a GIS-based fuzzy logic platform using AND operator. Six thematic layers are generated (four from petrophysics; i.e. V_{sh}, ϕ_{Eff}, K, S_w, and two from seismic analysis; i.e. AI, and SA) and reclassified to five classes for the B-sandstone reservoir identified as having the best hydrocarbon potentiality.

A fuzzy-based reservoir quality map was conducted for B-sandstone reservoir. The fuzzy prediction map shows that the middle-eastern portion zone is highly favourable for further HC exploitation (Figure 20). This zone showed consistently favourable behaviour on all the six constructed thematic layers. The final map was overlaid on the time structure map of the TSF and a prospective zone was identified and suggested for exploration. Fuzzy logic effectively integrated all the layers, and now a prospective area at the top of B-sandstone is proposed for further exploration in the field.

Acknowledgements

The authors would like to thank the RMOTC for providing data for this research. CGG and Schlumberger are also acknowledged for providing licences of the Hampson-Russell (CGG), Petrel and Interactive Petrophysics programs. The authors extend their sincere appreciation to the Deanship of Scientific Research at the King Saud University for funding the Prolific Research Group (PRG-1436–21).

References

Abd El Rahman, A., and Lashin, A., 2004, Evaluation of the basement reservoir rocks in some selected wells in north Gulf of Suez and south Sinai: *Annals of Geological Survey of Egypt*, **XXVII**, 459–477.

Al-Zuabi, Y., Al-Khaled, O., Abd-Rabu, K., Sulistiono, D., and Celma, R., 2011, Quantitative reservoir characterization through simultaneous inversion: a case study from the Burgan Field, Kuwait: 81st SEG Annual Meeting, San Antonio, SEG-2011–1719.

AlMuhaidib, A. M., Sen, M. K., and Toksoz, M. N., 2012, Integration of geology, rock physics, logs, and prestack seismic data for reservoir porosity estimation: *AAPG Bulletin*, **96**, 1235–1251. doi:10.1306/01021211083

Amaefule, J. O., Altunbay, M., Tiab, D., Kersey, D. G., and Keelan, D. K., 1993, Enhanced reservoir description using core and log data to identify hydraulic (flow) units and predict permeability in uncored intervals/wells: 68th Annual Technical Conference and Exhibition of the Society of Petroleum Engineers, 205–220.

Amigun, J., and Bakare, N., 2013, Reservoir evaluation of "Danna" field Niger delta using petrophysical analysis and 3D seismic interpretation: *Petroleum & Coal*, **55**, 119–127.

Anna, L. O., 2009, Geologic assessment of undiscovered oil and gas in the Powder River Basin Province, Wyoming and Montana. Digital Data Series DDS–69–U.

Archie, G. E., 1942, The electrical resistivity log as an aid in determining some reservoir characteristics: *Petroleum Transactions of AIME*, **146**, 54–62. doi:10.2118/942054-g

Asquith, G. B., Krygowski, D., and Gibson, C. R., 2004, *Basic well log analysis*: American Association of Petroleum Geologists.

Brown, A. R., 2004, *Interpretation of three-dimensional seismic data* (6th edition): AAPG and SEG.

Chambers, R. L., and Yarus, J. M., 2002, Quantitative use of seismic attributes for reservoir characterization: *CSEG Recorder*, **27**, 14–25.

Cheney, T. M., and Sheldon, R. P., 1959, Permian stratigraphy and oil potential, Wyoming and Utah, *in* N. C. Williams, ed., *Guidebook to the geology of the Wasatch and Uinta Mountains Transition Area*: Intermountain Association of Petroleum Geologists, Tenth Annual Field Conference, 90–100.

Chopra, S., and Marfurt, K., 2006, Seismic attributes – a promising aid for geologic prediction: *CSEG Recorder*, **31**, 110–120.

Clayton, J. L., and Ryder, R. T., 1984, Organic chemistry of black shales and oils in the Minnelusa Formation (Permian and Pennsylvanian), Powder River Basin, Wyoming, *in* J. Woodward, F. F. Meissner, and J. L. Clayton, eds., *Hydrocarbon source rocks of the Greater Rocky Mountain region*: Rocky Mountain Association of Geologists, 231–244.

Contreras, A., Torres-Verdin, C., Chesters, W., Kvien, K., and Globe, M., 2005, Joint stochastic inversion of petrophysical logs and 3D pre-stack seismic data to assess the spatial continuity of fluid units away from wells: application to a Gulf-of-Mexico deep water hydrocarbon reservoir: 46th Annual Logging Symposium, Society of Petrophysicists and Well Log Analysts, 26–29 June 2005, New Orleans, Louisiana.

Cuddy, S. J., 1997, The application of fuzzy logic to petrophysics: 38th Annual Logging Symposium, Society of Petrophysicists and Well Log Analysts, 15–18 June 1997, Houston, Texas.

De Bruin, R. H., 1993, Overview of oil and gas geology of Wyoming, *in* A. W. Snoke, J. R. Steidtmann, and S. M. Roberts, eds., *Geology of Wyoming*: Geological Survey of Wyoming, Memoir No. 5, 836–873.

Dennen, K., Burns, W., Burruss, R., and Hatcher, K., 2013, Geochemical analyses of oils and gases, Naval Petroleum Reserve No. 3, Teapot Dome Field, Natrona County, Wyoming: USGS Open-File Report 2005–1275.

Doll, T. E., Luers, D. K., Strong, G. R., Schulte, R. K., Sarathi, P. S., Olsen, D. K., and Hendricks, M. L., 1995, An update of steam injection operations at Naval Petroleum Reserve No. 3, Teapot Dome field, Wyoming: a shallow heterogeneous light oil reservoir: SPE International Heavy Oil Symposium, 19–21 June 1995, Calgary, Alberta, Canada.

Dolton, G. L., and Fox, J. E., 1995, Powder River Basin Province (033), *in* D. L. Gautier, G. L. Dolton, K. I. Takahashi, and K. L. Varnes, eds., *1995 National Assessment of Oil and Gas Resources—Results, Methodology, and Supporting Data*: US Geological Survey Digital Data Series DDS-30, one CD-ROM, Release 2.

Duijndam, A. J. W., 1988, Bayesian estimation in seimic inversion. Part I: Principles: *Geophysical Prospecting*, **36**, 878–898. doi:10.1111/j.1365-2478.1988.tb02198.x

El-Mowafy, H., and Marfurt, K. J., 2008, Structural interpretation of the middle Frio Formation using 3D seismic and well logs: an example from the Texas Gulf Coast of the United States: *The Leading Edge*, **27**, 840–854. doi:10.1190/1.2954023

El-Naby, A. A., El-Aal, M. A., Kuss, J., Boukhary, M., and Lashin, A., 2009, Structural and basin evolution in Miocene time, southwestern Gulf of Suez, Egypt: *Neues Jahrbuch für Geologie und Palaontologie. Abhandlungen*, **251**, 331–353. doi:10.1127/0077-7749/2009/0251-0331

Encyclopedia Britannica, 2014. Teapot Dome scandal. Available at: http://www.britannica.com/EBchecked/topic/585252/Teapot-Dome-Scandal

Esri, 2011, Applying fuzzy logic to overlay rasters. Available at: http://help.arcgis.com/EN/ArcGISDesktop/10.0/Help/index.html#/Applying_fuzzy_logic_to_overlay_rasters/009z000000rv000000

Esri, 2012, ArcGIS resources. Available at: http://resources.arcgis.com/en/communities/imagery

Friedmann, S. J., and Stamp, V., 2006, Teapot Dome: site characterization of a CO_2-enhanced oil recovery and storage research site in eastern

Wyoming: *Environmental Geoscience*, **13**, 181–199. doi:10.1306/eg.01200605017

Friedmann, S., Nummedal, D., and Stamp, V., 2004, Science and technology goals of the Teapot Dome field experimental facility: The Fourth National Conference on Carbon Sequestration, Washington, D. C., 1–8.

Gardner, G. H. F., Gardner, L. W., and Gregory, A. R., 1974, Formation veloicty and density – the diagnostic basics for stratigraphic traps: *Geophysics*, **39**, 770–780. doi:10.1190/1.1440465

Jafri, M. K., Lashin, A., Ibrahim, E., and Naeem, M., 2016, Petrophysical evaluation of the Tensleep Sandstone formation using well logs and limited core data at Teapot Dome, Powder River Basin, Wyoming, USA: *Arabian Journal for Science and Engineering*, **41**, 223–247. doi:10.1007/s13369-015-1741-7

Kainz, W., 2010, *Fuzzy logic and GIS*: University of Vienna.

Larionov, V., 1969, *Radiometry of boreholes*: Nedra (Moscow).

Lashin, A., and Abd El Aal, M., 2004*a*, Juxtaposition and fault seal analysis of some mixed clastic reservoirs, Egypt: *Journal of the Egyptian Geophysical Society*, **2**, 165–184.

Lashin, A., and Abd El Aal, M., 2004*b*, Seismic data analysis to detect the depositional process environment and the structural framework of east central part of Gharib Province, Egypt: *Annals of Geological Survey of Egypt*, **XXVII**, 523–550.

Lashin, A., and El Din, S., 2013, Reservoir parameters determination using artificial neural networks: Ras Fanar field, Gulf of Suez, Egypt: *Arabian Journal of Geosciences*, **6**, 2789–2806. doi:10.1007/s12517-012-0541-6

Lashin, A., and El-Naby, A., 2014, Petrophysical, seismic structural and facies analysis of the Miocene reservoirs of East Morgan oil field, Gulf of Suez, Egypt: *Arabian Journal of Geosciences*, **7**, 3481–3504. doi:10.1007/s12517-013-1011-5

Lashin, A., El Shahat, W., and Sharaf, M., 2003, Formation evaluation of the Cenomanian and Lower Cretaceous rocks in the north eastern part of Sinai, Egypt: *Egyptian Journal of Geology*, **47**, 1297–1324.

Lashin, A., Al-Arifi, N., and Ashour, N. A., 2011, Evaluation of the ASL and Hawara formations using seismic-and log-derived properties, October Oil Field, Gulf of Suez, Egypt: *Arabian Journal of Geosciences*, **4**, 365–383. doi:10.1007/s12517-009-0065-x

Lashin, A., Zahra, H., Ibrahim, F., Serag Eldien, S., and Al-Bassam, A., 2014, Petrophysical and electrofacies analysis of Nullipore Reservoir, Ras Fanar Field, Gulf of Suez-Egypt: *Petroleum Science and Technology*, **32**, 1851–1860. doi:10.1080/10916466.2012.655874

Lashin, A., Bin Marta, E., and Mohamed Khamis, M., 2016, Characterization of the Qishn sandstone reservoir, Masila Basin-Yemen, using an integrated petrophysical and seismic structural approach: *Journal of African Earth Sciences*, **115**, 121–142. doi:10.1016/j.jafrearsci.2015.11.026

Latimer, R., Davison, R., and van Riel, P., 2000, An interpreter's guide to understanding and working with seismic-derived acoustic impedance data: *The Leading Edge*, **19**, 242–256. doi:10.1190/1.1438580

Lindseth, R. O., 1979, Synthetic sonic logs – a process for stratigraphic interpretation: *Geophysics*, **44**, 3–26. doi:10.1190/1.1440922

Lloyd, H. J. E., and Margrave, G. F., 2011, Comparison of low frequency seismic data to well logs – Hussar example: CREWES Research Report, Vol. 23, No. 72.

Mohamed, A., Ibrahim, E., and Sabry, A., 2013, Petrophysical characteristics of Wakar Formation, Port Fouad marine field, north Nile Delta, Egypt: *Arabian Journal of Geosciences*, **6**, 1485–1497. doi:10.1007/s12517-011-0446-9

Momper, J. A., and Williams, J. A., 1984, Geochemical exploration in the Powder River basin, *in* G. Demaison, and R. J. Murris, eds., *Petroleum geochemistry and basin evaluation*: American Association of Petroleum Geologists Memoirs 35, 181–191.

Morris, R., and Biggs, W., 1967, Using log-derived values of water saturation and porosity: 8th Annual Logging Symposium, Society of Petrophysicists and Well-Log Analysts, 12–14 June, Denver, Colorado.

Naeem, M., El-Araby, H. E., Khalil, M. K., Jafri, K. M., and Khan, F., 2015, Study of seismic and well data for porosity estimation using multi-attribute transforms: a case study of Boonsville Field, Fort Worth Basin, Texas, USA: *Arabian Journal of Geosciences*, **8**, 8777–8793. doi:10.1007/s12517-015-1806-7

Norland, U., 1996, Formalizing geological knowledge, with an example of modeling stratigraphy using fuzzy logic: *Journal of Sedimentary Research*, **66**, 689–698.

Pendrel, J., 2001, Seismic inversion – the best tool for reservoir characterization: *CSEG Recorder*, **26**, 18–24.

Pendrel, J., 2006, Seismic inversion – a critical tool in reservoir characterization: *Scandinavian Oil-Gas Magazine*, **5/6**, 19–22.

Pendrel, J., and Van Riel, P., 1997, Methodology for seismic inversion and modeling: a western Canadian reef example: *CSEG Recorder*, **22**, 105–109.

Roth, M., Emanuel, J., and Anderson, T., 2005, Better understanding Wyoming tight gas reservoirs through co-visualization and analysis of 3D seismic, VSP and engineering data – Teapot Dome, Powder River Basin: 3D Seismic Symposium, Rocky Mountain Association of Geologists/Denver Geological Society, 1–5.

Russell, B., 2005, Strata workshop: theory and exercises in seismic inversion and AVO: unpublished lecture notes.

Russell, B., and Hampson, D., 2006, The old and the new in seismic inversion: *CSEG Recorder*, **12**, 5–11.

Russell, B., and Toksöz, M. N., 1991, Comparison of poststack seismic inversion methods: 1991 SEG Annual Meeting, Houston, Texas, SEG-1991-0876.

Savic, M., VerWest, B., Masters, R., Sena, A., and Gingrich, D., 2006, *Elastic impedance inversion in practice*: ARCO Alaska Inc.

Schlumberger, 1986, Schlumberger well services. Houston, Texas.

Schlumberger, 1995, Log Interpretation, Principles/Applications. Houston, Texas.

Schlumberger, 1991, Charts. Schlumberger educational services. Houston, Texas.

Schwartz, B. C., 2006, Fracture pattern characterization of the Tensleep Formation, Teapot Dome, Wyoming: M.Sc. thesis, West Virginia University.

Serra, O., Westaway, P., and Abbott, H., 1984, *Fundamentals of well-log interpretation*: Elsevier.

Sheldon, R. P., 1967, Long-distance migration of oil in Wyoming: *The Mountain Geologist*, **4**, 53–65.

Shrestha, R. K., and Boeckmann, M. K., 2002, Stochastic seismic inversion for reservoir modelling: SEG Annual Meeting, October 2002.

Sneider, R. M., and King, H. R., 1984, Integrated rock-log calibration in the Elmworth Field, Alberta, Canada: part I: reservoir rock detection and characterization, *in* J. A. Masters, ed., *Elmworth – case study of a deep basin gas field*: AAPG Memoir, **38**, 205–214.

Strickland, J. W., 1958, Habitat of oil in the Powder River basin: 13th Annual Field Conference, Wyoming Geological Association, 132–147.

Thom, W. T., Jr, and Spieker, E. M., 1931, The significance of geologic conditions in Naval Petroleum Reserve No. 3, Wyoming, with a section on the waters of the Salt Creek-Teapot Dome uplift by Herman Stabler: US Geological Survey, Paper 163.

Ulrych, T. J., Sacchi, M. D., and Woodbury, A., 2001, A Bayes tour of inversion: a tutorial: *Geophysics*, **66**, 55–69.

Vargas-Meleza, L., Megchun, J., and Vazquez, G., 2004, Petrophysical properties estimation by integrating AVO, seismic inversion and multiattribute analysis in a 3-D volume of Playuela, Veracruz: AAPG International Conference, 24–27 October, Cancun, Mexico.

Veeken, P. C. H., and Da Silva, M., 2004, Seismic inversion methods and some of their constraints: *First Break*, **22**, 44–70.

Walden, A., and White, R., 1998, Seismic wavelet estimation: *IEEE transactions on Geoscience and Remote Sensing*, **36**, 287–297. doi:10.1109/36.655337

Wang, Z., 2001, Fundamentals of seismic rock physics: *Geophysics*, **66**, 398–412.

Wegemann, C. H., 1911, The Salt Creek oil field, Wyoming: *US Geological Survey Bulletin*, **452**, 37–38.

Zadeh, L., 1965, Fuzzy sets: *Information and Control*, **8**, 338–353. doi:10.1016/S0019-9958(65)90241-X